

General Disclaimer

One or more of the Following Statements may affect this Document

- This document has been reproduced from the best copy furnished by the organizational source. It is being released in the interest of making available as much information as possible.
- This document may contain data, which exceeds the sheet parameters. It was furnished in this condition by the organizational source and is the best copy available.
- This document may contain tone-on-tone or color graphs, charts and/or pictures, which have been reproduced in black and white.
- This document is paginated as submitted by the original source.
- Portions of this document are not fully legible due to the historical nature of some of the material. However, it is the best reproduction available from the original submission.

(NASA-CR-121142) THRUST VECTORING SYSTEMS
Final Report (Hughes Research Labs.)
82 p HC \$6.25 CSCL 21C

N73-17816

Unclass

G3/28 63409

THRUST VECTORING SYSTEMS

FINAL REPORT

DECEMBER 1972



BY

ION DEVICE PHYSICS DEPARTMENT STAFF

HUGHES RESEARCH LABORATORIES

3011 MALIBU CANYON ROAD
MALIBU, CALIFORNIA 90265

PREPARED FOR

NATIONAL AERONAUTICS AND SPACE ADMINISTRATION
NASA LEWIS RESEARCH CENTER
CONTRACT NAS 3-15385
WALTER LATHAM, PROJECT MANAGER

1. Report No. NASA CR-121142		2. Government Accession No.		3. Recipient's Catalog No.	
4. Title and Subtitle THRUST VECTORING SYSTEM				5. Report Date December 1972	
				6. Performing Organization Code	
7. Author(s) H.J. King, <u>et al.</u>				8. Performing Organization Report No.	
9. Performing Organization Name and Address Hughes Research Laboratories 3011 Malibu Canyon Road Malibu, California 90265				10. Work Unit No.	
				11. Contract or Grant No. NAS 3-15385	
12. Sponsoring Agency Name and Address National Aeronautics and Space Administration Lewis Research Center 21000 Brookpark Road Cleveland, Ohio 44135				13. Type of Report and Period Covered Contractor Report - Final	
				14. Sponsoring Agency Code	
15. Supplementary Notes Project Manager: Walter Latham, NASA-Lewis Research Center, Cleveland, Ohio					
16. Abstract The design, fabrication, and testing of thrust vectorable ion optical systems capable of controlling the thrust direction from both 5- and 30-cm diameter ion thrusters is described. Both systems are capable of greater than 10^0 thrust deflection in any azimuthal direction. The 5-cm system is electrostatic and hence has a short response time and minimal power consumption. It has recently been tested for more than 7500 hours on an operational thruster. The 30-cm system is mechanical, has a response time of the order of 1 min, and consumes less than 0.3% of the total system input power at full deflection angle.					
17. Key Words (Suggested by Author(s))				18. Distribution Statement	
19. Security Classif. (of this report) Unclassified		20. Security Classif. (of this page) Unclassified		21. No. of Pages 74	22. Price* \$3.00

* For sale by the National Technical Information Service, Springfield, Virginia 22151

FOREWORD

The work described herein was performed in the Ion Device Physics Department of the Research Laboratories of the Hughes Aircraft Company in Malibu, California. This department is managed by Mr. J.H. Molitor. The work was performed under Contract NAS 3-15385, managed by Mr. W. Latham of NASA Lewis Research Center. Major technical contributors to this effort were:

H.J. King	Project Manager, ion optics design and evaluation
D. Schnelker	Mechanical Design
J.W. Ward	Ion Optical System Testing, analytical studies
C. Dulgeroff	5-cm Optics Evaluation
R. Vahrenkamp	30-cm Optics Evaluation.

TABLE OF CONTENTS

	LIST OF ILLUSTRATIONS	vii
	ABSTRACT	ix
	SUMMARY	xi
I	INTRODUCTION	1
II	PART I — 5-cm SYSTEM	5
	A. Program Outline	5
	B. Mechanical Design — 5-cm System	6
	C. System Performance Tests	17
	D. Conclusion	48
III	PART II — 30-cm SYSTEM	51
	A. Program Outline	51
	B. Mechanical Design — 30-cm System	52
	C. System Performance Evaluation	58
	D. Conclusion	66
	REFERENCES	69
	APPENDIX	71

LIST OF ILLUSTRATIONS

Fig. 1.	5 cm Thrust Vectoring Grid System	9
Fig. 2.	Accelerometer Positions, 5 cm Thrust Vectoring Optics	11
Fig. 3.	Schematic of different Pole Piece Geometries Tested	18
Fig. 4.	Representative Beam Profiles	19
Fig. 5.	Perveance Curve for Three-Pole Piece Configurations	21
Fig. 6.	Measured Undelected Accel Currents as a Function of Beam Current	24
Fig. 7.	Accelerator Current Versus Deflection Voltage $I = 25$ mA	25
Fig. 8.	Accelerator Current Versus Deflection Voltage $I = 30$ mA	25
Fig. 9.	Accelerator Current Versus Deflection Voltage $I = 35$ mA	26
Fig. 10.	Perveance Curve	27
Fig. 11.	Aperture Dimensions of Dual Grid Electrostatic Deflection System	30
Fig. 12.	Functional Diagram of Deflection Power Conditioning	32
Fig. 13.	Measured Perveance Curves for 0.125 in. Diameter Screen Holes, 0.105 Accel Apertures, 0.030 in. Grid Spacing	34
Fig. 14.	Accel Current Versus Ion Beam Current	35
Fig. 15.	Discharge Energy per Ion Versus Propellant Utilization	37
Fig. 16.	Deflection Angle Versus X-Deflection Voltage ($I_t = 20$ mA)	39
Fig. 17.	Deflection Angle Versus X-Deflection Voltage ($I_t = 25$ mA)	40

Fig. 18.	Deflection Angle Versus X-Deflection Voltage ($I_t = 30$ mA)	41
Fig. 19.	Deflection Angle Versus X-Deflection Voltage ($I_t = 34$ mA)	42
Fig. 20.	Screen Translation as Function of Total Input Power for Different Spring Orientation	54
Fig. 21.	Schematic of Expanding Fluid Motion Generator	55
Fig. 22.	30-cm Thrust Vectoring System	56
Fig. 23.	Thrust Vectoring Actuator Concept	57
Fig. 24.	Measured Beam Deflection as Function of Screen Translation	59
Fig. 25.	Ion Optical Systems Thermal Test Results	62
Fig. 26.	Relationship Between Ion Beam Current, Actuator Temperature, and Actuator Heater Power	63
Fig. 27.	Extraction SN503 Y-Axis Bench Test	64
Fig. 28.	Thrust Vector Motion as Beam Increases	65
Fig. 29.	Results as Actuators are Heated after Ambient Temperature is reached	67
Fig. 30.	Typical Beam Profile	68
Fig. 31.	Tabulation of Measured Beamlet Sizes for Two Grid Spacings	72
Fig. 32.	Measured Beamlet Size Versus Radius for Thrust Vector Optics with Square-Type Screen Aperture for Two Grid Spacings	73

ABSTRACT

The design, fabrication, and testing of thrust vectorable ion optical systems capable of controlling the thrust direction from both 5- and 30-cm diameter ion thrusters is described. Both systems are capable of greater than 10° thrust deflection in any azimuthal direction. The 5-cm system is electrostatic and hence has a short response time and minimal power consumption. It has recently been tested for more than 7500 hours on an operational thruster. The 30-cm system is mechanical, has a response time of the order of 1 min, and consumes less than 0.3% of the total system input power at full deflection angle.

SUMMARY

Both 5- and 30-cm thrust vectoring systems have been designed, fabricated, and extensively tested under this program. The 5-cm system employs an interlocking matrix of electrodes in the accelerator that is positioned so a transverse electrostatic force can be applied to each beamlet as it is accelerated. This gives high speed of response (<1 msec), precise pointing accuracy, and requires no moving parts. The report describes in detail the effect of the ion optical system on the thruster performance, the calibration curves for deflection versus voltage, and the results of mechanical vibration tests on the ion optical system. A deflection system produced under this contract has successfully completed 7500 hours of testing at deflection angles up to 10° at the NASA Lewis Research Center as part of an ongoing thruster test. It is considered ready for flight application.

The 30-cm thruster system employs a mechanically translating screen electrode system. It was not possible to extend the 5-cm electrostatic technology to the larger thruster because of the increased complexity resulting from the much larger number of apertures in the 30-cm system (10^4 apertures compared to 10^2 in the 5-cm system). Two mechanical designs were implemented and tested. Each produced 10° deflection angles with no degradation in thruster efficiency and minimal increase in system weight. Neither design was structurally qualified. Since each type of actuator was thermally controlled, there was an interaction with the ambient temperature of the thruster shell that proved difficult to compensate. While the thrust deflection principle was proven in 30-cm size, it is desirable to improve the actuator system prior to finalizing a flight design.

SECTION I

INTRODUCTION

Mercury electron bombardment ion thrusters provide a number of technical and financial system advantages when used for both primary propulsion of space vehicles or attitude control and stationkeeping of synchronous satellite¹⁻³. It is necessary to control the precise direction of the thrust vector in each system to compensate for initial misalignment of the thruster, changes in thrust orientation during the mission, or to control the attitude of the vehicle with respect to some fixed reference, such as the earth or the sun. Several means of thrust vector control by conventional or mechanical means that move the entire thruster or thruster array have been proposed. The goal of the work reported here was to evolve means of controlling the direction of the ion beam from a fixed thruster, thereby eliminating the weight, power, and complexity of auxiliary vectoring devices.

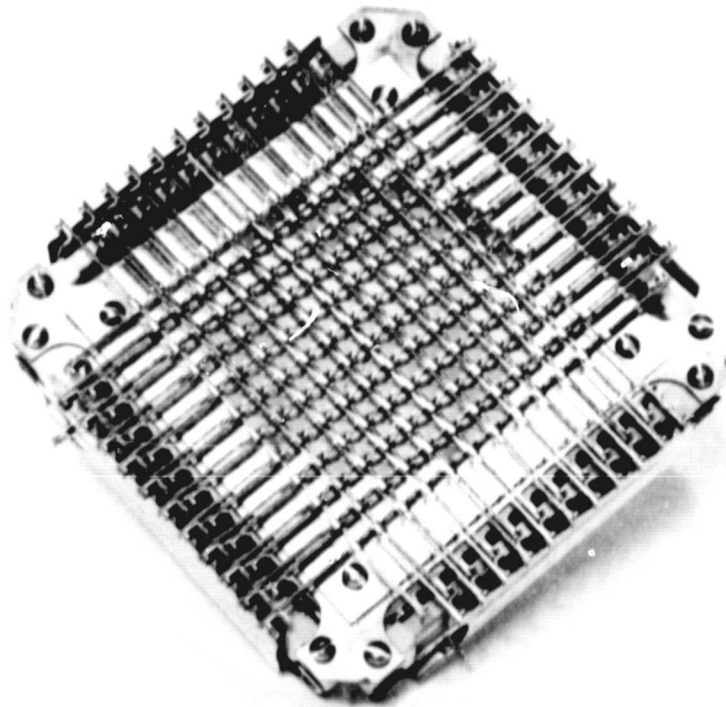
Successful prototype hardware was designed and tested under a preceding contract, NAS 3-14058, which also compared possible alternative thrust vectoring techniques and surveyed previous activity in this area.

During the present contract, thrust vectoring optics for both 5- and 30-cm ion thrusters were constructed and tested. These optics interface directly with thrusters of these sizes constructed at HRL (under Contracts NAS 3-15483 and NAS 3-14040) that have been employed as test vehicles for the optics system. Deflection angles of $\pm 10^\circ$ to any azimuthal direction have been demonstrated for both thruster sizes. This should be adequate for all applications proposed to date.

The work described here is important because it describes the only thrust vectoring system of any type for a 30-cm thruster and the only electrostatic multiaperture deflection system that have been built and tested.

PRECEDING PAGE BLANK NOT FILMED

M8388



5cm THRUST VECTORING SYSTEM

SECTION II

PART 1 - 5-cm SYSTEM

A. PROGRAM OUTLINE

The fundamental principles on which the 5-cm electrostatic thrust vector grids are based were verified in an earlier contract.* The goal of the work reported here was to modify the basic design as required to demonstrate both mechanical integrity during launch and long, stable operational lifetime. The major steps in this procedure are as follows:

1. The design and fabrication of the improved extraction system discussed in the Final Report on Contract NAS 3-14058 was completed.
2. The structural qualification of this prototype was successful.
3. Two additional units incorporating minor design and assembly improvements were fabricated. These electrode systems were delivered to NASA LeRC for parametric and life testing.
4. A series of experiments were conducted to evaluate both the performance of the electrodes themselves and the effect that parametric changes of screen pole piece design and other minor discharge chamber modifications would have on over-all system performance.
5. The results of the above tests and of life tests conducted at LeRC were discussed in a design review held at LeRC. Agreement was reached on a design for the final electrode system that conservatively assured 10^4 hours of operation at the expense of a small reduction in over-all efficiency.
6. Several sets of electrodes of this final design were fabricated and tested both at LeRC and HRL. In a continuing test at LeRC, one set has accumulated 7500 hours of operation (as of December 1972), without significant change in performance or

* Contract NAS 3-14058 from LeRC, 1971.

appearance, as seen through a high power telescope looking into the test facility. A second set was extensively performance-mapped, as reported elsewhere in this report. A third set was successfully qualified structurally as part of the SIT-5 thruster package fabricated and tested under Contract NAS 3-15483.

B. MECHANICAL DESIGN - 5-cm SYSTEM

1. Design Details - 5-cm Deliverable Hardware

The basic technique of electrostatically deflecting the beam consists of imposing a transverse electric field across the ion beam in the region of the negative accelerator electrode prior to neutralization. This technique was applied first to cesium contact thrusters of both single, circular aperture and linear-strip configurations. Extension of this concept to bombardment thrusters (whose ion extraction system consists of a two-dimensional array of circular apertures) is made mechanically difficult, because each aperture in the accelerator must contain four deflection plates electrically isolated from each other.

A practical design which has satisfied all electrical constraints is the so-called "eggcrate" structure developed at HRL, that is assembled from interlocking strip electrodes. Each aperture is bounded by the necessary four electrically independent electrodes. The individual strips are interconnected at the periphery of the electrode. The screen is a sheet of molybdenum drilled by conventional techniques to provide 0.318-cm diameter apertures on 0.445-cm centers in a square pattern. The accelerator consists of a number of notched strip electrodes attached to four orthogonal ceramic blocks by an array of leaf springs. The electrodes themselves are attached to the springs in such a way that the electrodes are locked in place and held under a light tension that maintains their position and alignment under varying thermal and dynamic loads.

This system has been subjected to shake and shock tests without incurring physical damage. The high degree of structural integrity is due to the fact that the electrodes themselves are very light and generate little force even at high G loads. Furthermore, the interlocking structure limits the amplitude of vibration to less than 0.05 cm, thus preventing deformation that would exceed the yield point.

The first grid system delivered to NASA LeRC under this contract (S/N 201) was identical to the final system fabricated for the previous Contract NAS 3-14058. The minor problems that became apparent during assembly of this system were corrected with minor design changes. These modifications are listed below with the serial number of the grid assembly where the change was implemented.

- a. Modification of spring strip bending die to make an accurate 90° bend necessary for improved alignment (S/N 202).
- b. Improvement of bend on end of accel strips to more closely conform to cross section of spring finger. (S/N 202).
- c. Difficulty in alignment of spring strip-insulator bars was reduced by providing more screw clearance and by making an assembly fixture to align the bars in the proper position. (S/N 202).
- d. Spotwelding of sputter shields was eliminated by redesigning to mount from existing screws at screen positive potential (S/N 202).
- e. Electrical termination was made more convenient by bending a portion of the spring strips outward and providing a screw hole for lead attachment (S/N 202).
- f. Electrode spacing tolerance 0.076/0.090 cm reduced to 0.063/0.076 cm to improve clearance between strips and notches (S/N 203).
- g. Nonuniformity of accel strip straightness was improved by adding stiffening rib to strips (S/N 203).

Grid system S/N 202 was used for the structural integrity test described in the next section. S/N 203 was delivered to NASA LeRC for parametric life testing. After several series of experiments were conducted to evaluate the performance of the grid systems, a design review was held at NASA-LeRC and the following changes were made in the mechanical design to maximize the expected lifetime of the grid system and assure 10^4 hours of deflected operation:

- a. The accel strip thickness was increased from 0.01 cm to 0.05 cm. This change to thicker strips reduced the accel aperture from 0.343 cm to 0.267 cm, since the number of holes and center-center spacing remained the same.
- b. An improved accel strip mounting scheme was incorporated at this time. In addition, a sputter shield was added at each point where the accel strips intersect to reduce charge exchange erosion that became evident during extended life tests at NASA LeRC.

The final grid system design is shown in Fig. 1. The dimensions are listed in Table I.

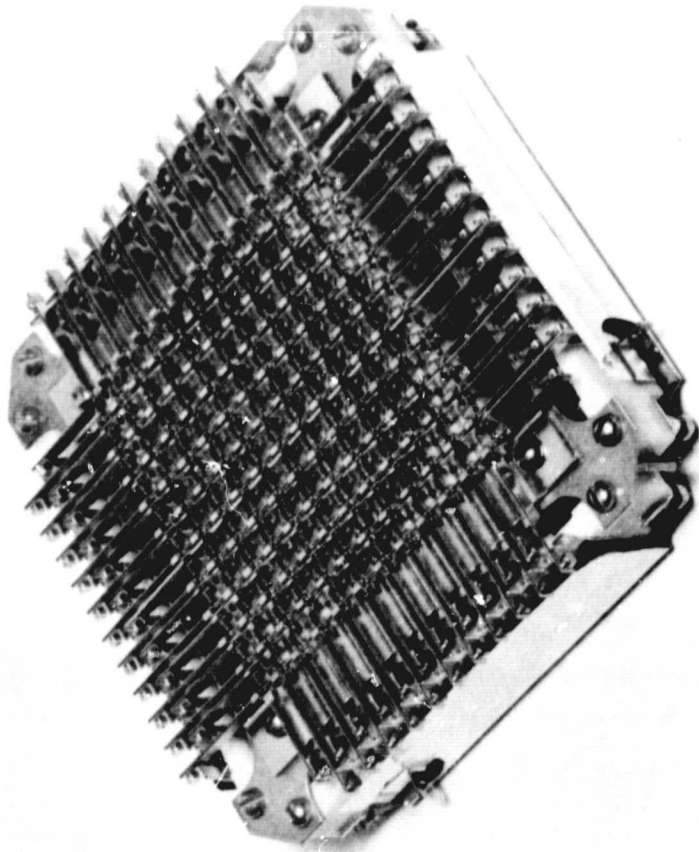
TABLE I

Dimensions of 5-Cm Dual Grid Electrostatic System

Number of Holes	89
Screen aperture diameter	0.318 cm
Center-center spacing	0.444 cm
Accel aperture size	0.267 cm
Screen thickness	0.051 cm
Accel thickness	0.254 cm
Screen-accel spacing	0.076 cm

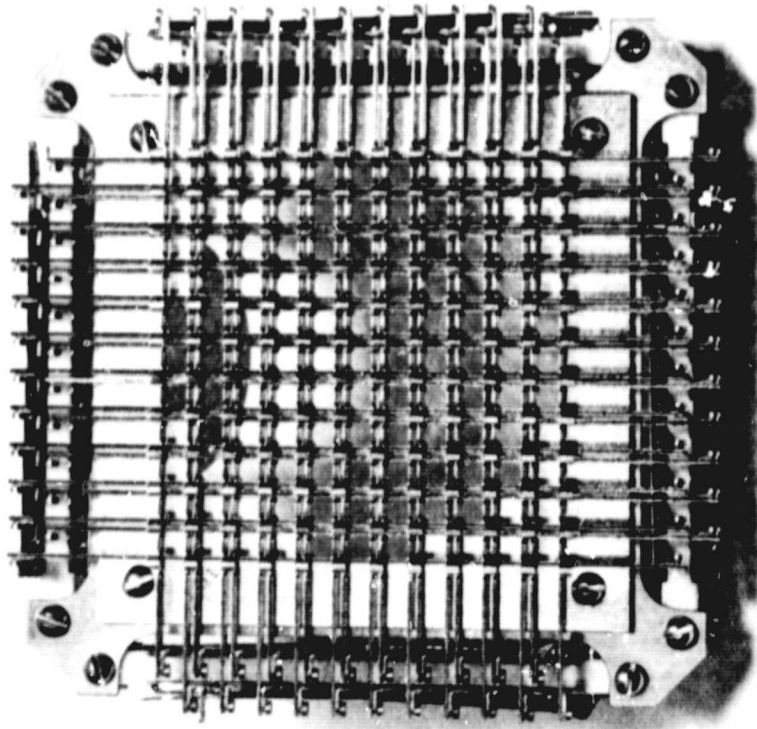
T798

M8332



(a)

M8333



(b)

Fig. 1. 5 cm Thrust Vectoring Grid System.

2. Structural Test Results - 5-cm Grid System

a. Test of Prototype System

The Thrust Vectoring System S/N 202 first was subjected to the specified qualification level vibration and shock testing. The grid system was then subjected to a series of sinusoidal vibration tests at levels well above those anticipated in normal service to determine the margin of safety in the design and the failure limit of the unit. This test program was conducted at the HAC Space Simulation Laboratory, El Segundo, California, during the period June 28-30, 1971.

The thrust vectoring system was tested in the three principal axes of the unit, of which one is parallel to the thrust axis, by applying and controlling the shock and vibration levels at the interface of the unit and the vibration fixture. The applied vibration levels were controlled by the average of two accelerometers located 180° apart, while the shock input was controlled using a single accelerometer. Cross axes response at the fixture-thruster interface was monitored during all tests by two accelerometers with their axes mutually perpendicular to the axis of excitation and to each other.

Accelerometers were located on the unit (to record the response of the vectoring grid) and on the structure supporting the vectoring grid. These response accelerometers (shown in Fig. 2) were recorded on magnetic tape for all qualification vibration and shock tests. The electrical continuity of the vectoring grid was also monitored for each test throughout the test program. This was accomplished by using a circuit to record on oscillograph paper any shorting of adjacent grids during testing. The criterion for failure was a permanently shorted circuit following test exposure. Shock test Nos. S1 through S7 were tested to the levels exceeding the qualification requirements by approximately 70%. This overtesting resulted from an incorrect calibration while setting up the shock pulse. The error was corrected and tests S8 through S18 were within the allowable tolerance.

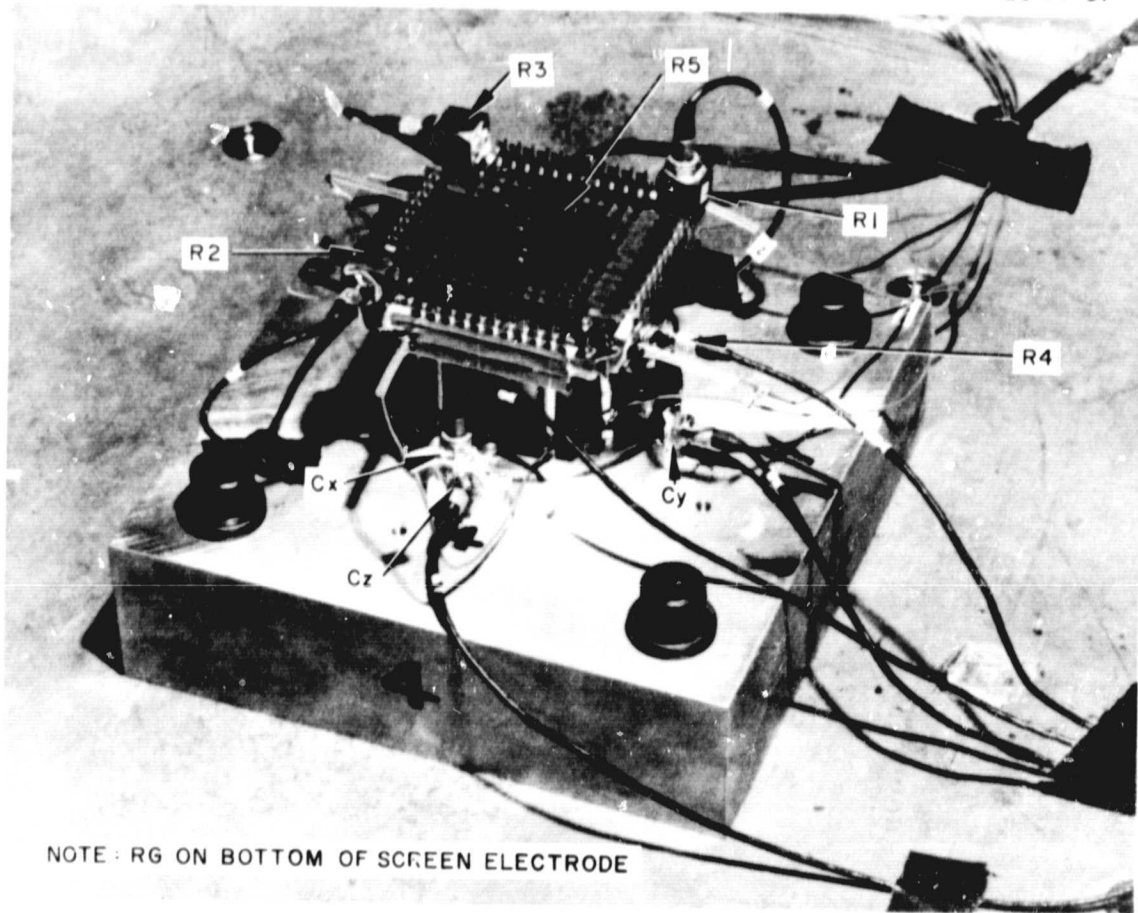


Fig. 2. Accelerometer Positions, 5 cm Thrust Vectoring Optics.

The Thrust Vectoring System was tested to the levels presented in Tables V through VIII in the sequence of Tables II through IV.

TABLE II
Vibration - Part I
Sinusoidal and Random Qualification Level

Test No.	Axis	Type of Test
1	Y	Low level (1.0 g) sinusoidal
2	Y	Qualification level sinusoidal
3	Z	Low level (1.0 g) sinusoidal
4	Z	Qualification level sinusoidal
5	X	Low level (1.0 g) sinusoidal
6	X	Qualification level sinusoidal
7A	X	-3dB random equalization
7	X	Qualification level random
8A	Z	-3dB random equalization
8	Z	Qualification level random
9	Y	Qualification level random

T799

TABLE III
Shock Test

Test No.	Axis	Type of Test
S1-S3	+Y	Qualification level
S4-S6	-Y	Qualification level
S7-S9	+Z	Qualification level
S10-S12	-Z	Qualification level
S13-S15	+X	Qualification level
S16-S18	-X	Qualification level

T800

TABLE IV

Vibration - Part II
Elevated Level Sinusoidal

Test No.	Axis	Type of Test
10	X	50% of elevated level
11	X	75% of elevated level*
12	Z	50% of elevated level
13	Z	75% of elevated level
14	Z	100% of elevated level
15	Y	50% of elevated level
16	Y	75% of elevated level
17	Y	100% of elevated level

*The limit of the vibration exciter was reached at 60% of the X-axis elevated level.

T801

TABLE V

Sinusoidal Vibration - Part I
Qualification Level Sinusoidal Vibration Test Specification

Frequency (Hz)	Level
5 - 19	0.5 in. double amplitude
19 - 2000	9.0 g's (0-peak)

T802

TABLE VI

Random Vibration Test Specification

Frequency (Hz)	Power Spectral Density
20 - 340	0.11 g ² /Hz
340 - 400	Up 12 dB/octave
400 - 2000	0.22 g ² /Hz
Over-all level: 19.9 grms Duration: 5.4 min/axis	

T803

TABLE VII

Shock Pulse Environment

Pulses	Peak Amplitude	Duration
+3 and 3- half sine pulses in each of the three orthogonal directions	30 g's	8 milliseconds
Total: 18		

T804

TABLE VIII

Sinusoidal Vibration - Part II
Elevated Sinusoidal Vibration Test Levels

	Frequency (Hz)	Level
Lateral axes (Y, Z)	5 - 19	0.5 in. double amplitude
	19 - 250	9.0 g's (0-peak)
	250 - 600	30.0 g's (0-peak)
	600 - 1200	70.0 g's (0-peak)
	1200 - 2000	9.0 g's (0-peak)
Thrust axis (X)	5 - 19	0.50 in. double amplitude
	19 - 250	9.0 g's (0-peak)
	250 - 500	100.0 g's (p-peak)
	500 - 2000	9.0 g's (0-peak)
Sweep rate: 2 octaves/min		

T805

Sinusoidal vibration tests were run in each axis to determine the fragility level of the test item. The fragility level was determined by subjecting the test item to 50, 75, and 100% of the acceleration levels above 9.0 g's. In the case of the X axis, the acceleration limit of the vibration exciter was reached at 60% of the specified 100 g level, and therefore the 100% test was deleted. After each test, an inspection of the test item was made and the oscillograph record of grid electrical continuity was reviewed to determine if a structural or functional failure had occurred. The grid network shorted permanently during test No. 15 (50% of maximum lateral test level, Y axis); however, the remaining two tests (Nos. 16 and 17) were run to complete the series.

b. Test of Final System

A system of the final configuration illustrated in Fig. 1 was integrated mechanically with the SIT-5 thruster as part of Contract NAS 3-15483 for both performance and structural tests. While these have been reported in detail in the final report under that contract, they are noted here to verify the integrity of the system in its actual system environment.

The complete SIT-5 system was subjected to structural tests similar to those described for the electrodes above. Even with the amplification factor introduced by the system the only structural damage incurred in the ion extraction system was the failure of the sputter shields at their mounting points and loosening of one pin that had been improperly brazed. The ends of the sputter shields were increased in thickness to provide more rigidity and the brazing procedure was modified slightly to effectively solve these two weaknesses as proven in subsequent tests.

Conclusions

The Thrust Vectoring System has been successfully qualified to the required vibration test levels and has demonstrated structural

adequacy specified by the design requirements. After the qualification level tests, the vectoring grid network showed no permanent shorting.

Considering the overtesting during 7 of the 18 shock pulses applied to the test item, no apparent damage was noted by close physical inspection of the structure and continuity tests showed no permanent shorting of the grid network.

C. SYSTEM PERFORMANCE TESTS

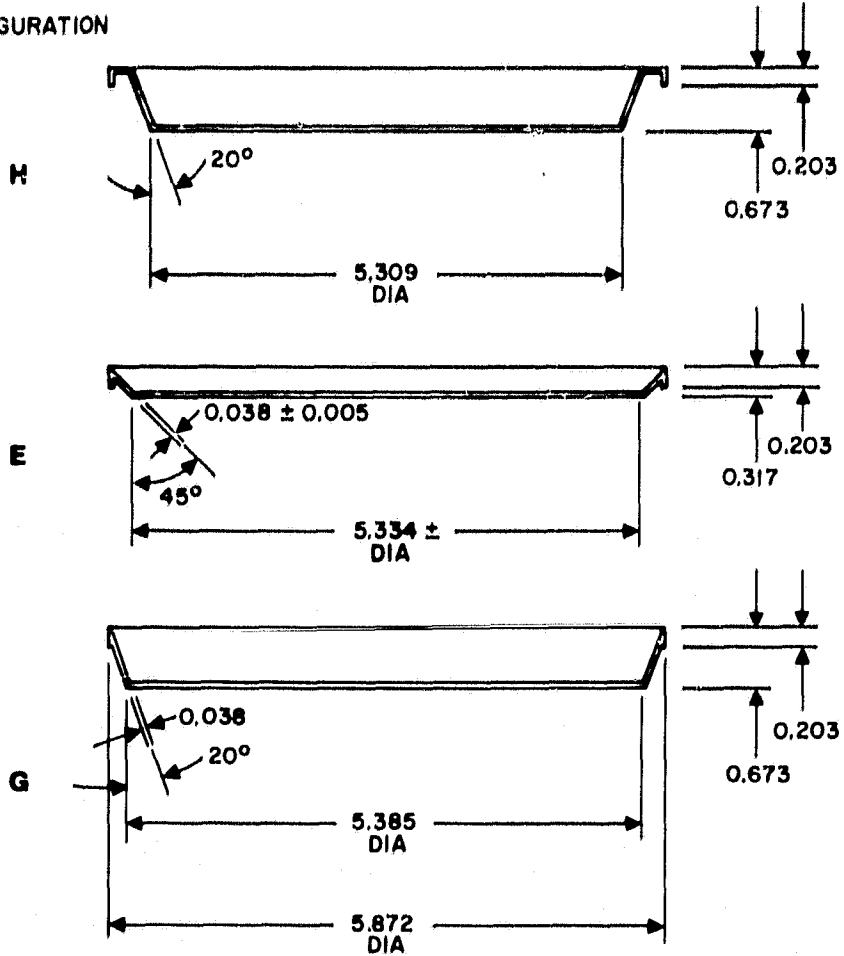
1. Short Term Tests

In arriving at a final optimized thrust vector optics design, a number of short term tests were performed with the goal of maximizing the lifetime of the deflectable optics by reducing the ion impingement currents to the lowest possible values. This was accomplished in two steps: first, by adjusting the shape of the screen magnetic pole piece and secondly, by a parametric study of different ion optics element geometries. The latter experiments included screen electrode modifications, grid spacings, and accel strip geometries. After these short term tests, the final design chosen was performance-mapped during a 150-hour test which demonstrated the deflection optics lifetime had been increased without sacrificing the deflection sensitivity of previous designs.

a. Screen Pole Piece Variations

The initial series of experiments were conducted with conventional optics (dimensions in Table IX) to find a pole piece geometry to produce a uniform beam profile. The three most promising pole piece configurations that were tested are shown in Fig. 3 and are designated E, H, and G. All of them produced a fairly uniform beam profile at a fixed z position. A representative beam profile for this series of experiments is shown using the H configuration in Fig. 4 for a beam current of 40 mA at $V_+ = 1200$ V and

CONFIGURATION



ALL MEASUREMENTS IN cm

Fig. 3. Schematic of Different Pole Piece Geometries Tested.

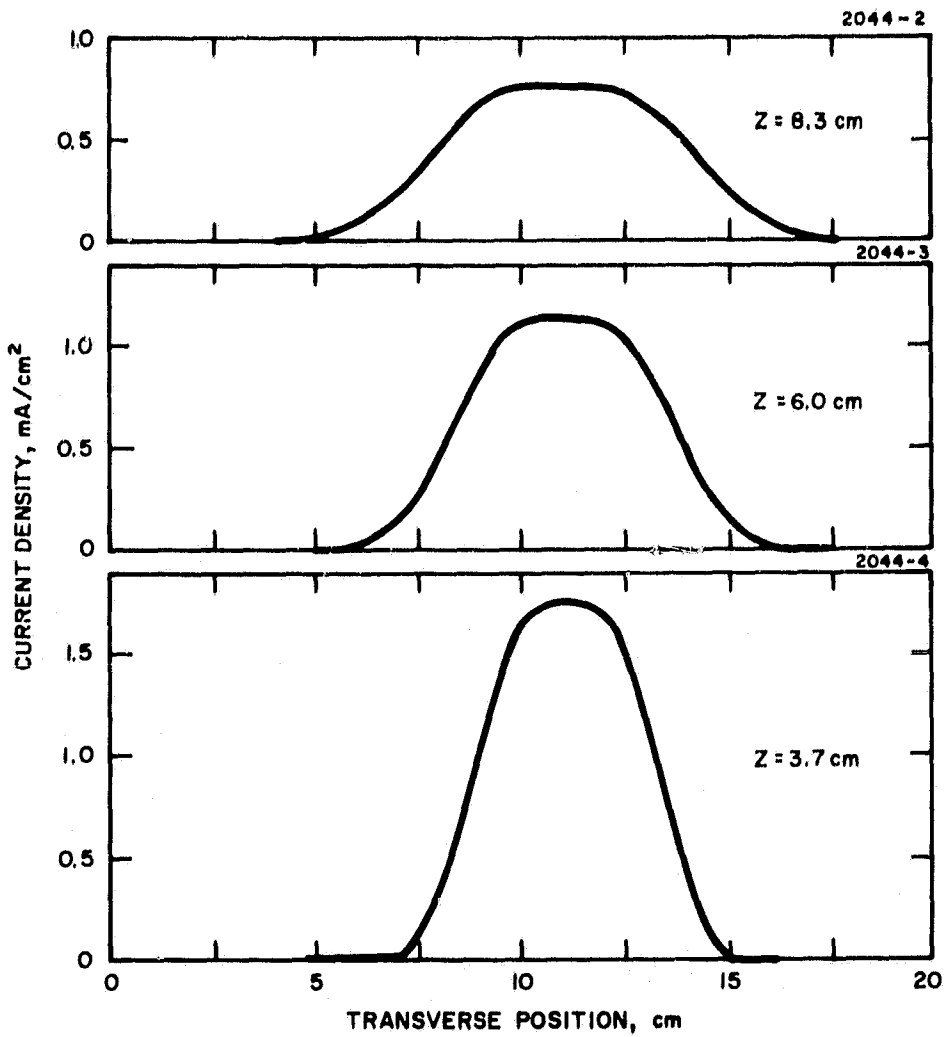


Fig. 4. Representative Beam Profiles.

TABLE IX

Parameters of Conventional Optics Used for Screen Pole
Piece Variations

Square Pattern 89 holes	
Screen Aperture dia.	0.391 cm
Screen Thickness	0.050 cm
Accel Aperture dia.	0.345 cm
Accel Thickness	0.127 cm
Screen-Accel Spacing	0.119 cm
Center to Center Spacing	0.444 cm

T806

$V_ = 1000$ V. A perveance curve for the three different screen pole piece variations tested was taken under similar operating conditions and is shown in Fig. 5. It is seen that configurations H and G have essentially the same limiting perveance, while configuration E clearly is lower. Thus, it is inferred that configurations H and G are producing a flatter beam profile, indicating that the perveance curve with a plot of accel current as a function of total voltage is a more sensitive indicator of the beam shape than the beam profiles described above.

This series of tests indicated the following:

1. The nearly identical beam profiles measured for the different pole piece configurations show that the thruster beam profile is relatively insensitive to pole piece variation.
2. Using the onset of the accel current increase when taking a perveance curve as a criterion of plasma uniformity, pole piece configuration H and G are substantially equal and clearly superior to configuration E.

b. Ion Optical Geometry Investigations

A summary of the five different ion optical geometries that were evaluated to provide comparative operating data is shown in

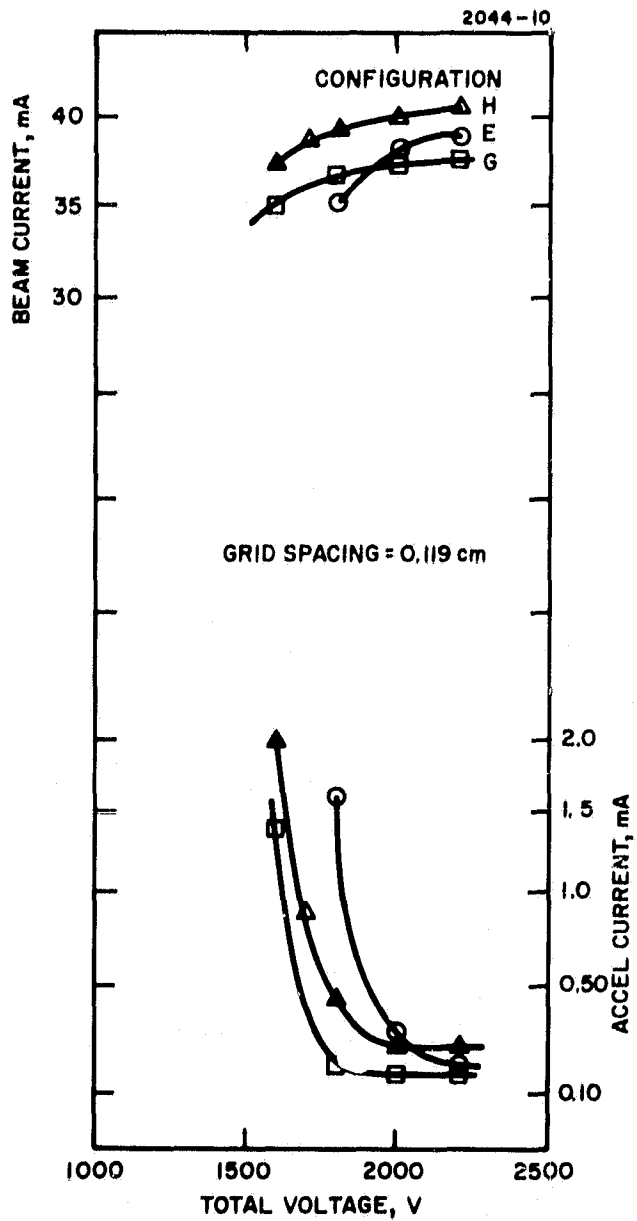


Fig. 5. Perveance Curve for Three-Pole Piece Configurations.

Table X. The first four configurations used the standard thrust vector optics of the same type previously delivered to LeRC under Contract NAS 3-14058. These optics have a deflection structure 0.254 cm long constructed of 0.0127 cm wide strips forming 0.343 cm² apertures while the last configuration (and the final design) used 0.267 cm² apertures formed by 0.051 cm wide strips. The first four configurations used the type G pole piece configuration, while the fifth configuration used the type H configuration. All of these tests included measurements of the accel drain current as a function of deflection voltage for different beam current, and measurements of the optics perveance for different beam currents. This data is summarized in Table X. Figure 6 shows the dependence of the undeflected accel current as a function of beam current for a total voltage of 2200 V. This curve shows that the resultant undeflected accelerator currents increase approximately linearly with beam current. Approximately 75% of this current is calculated to be charge exchange current, which is also shown plotted in Fig. 6.

The difference between the measured and calculated current is thought to be due to secondary electrons which would increase this component.

The total measured accel current is plotted versus the deflection voltage for nominal beam currents of 25-30, and 35 mA in Figs. 7 through 9. At a beam current of 35 mA, a sharp decrease in accel drains as the total voltage is raised from 2000 to 2400 V. For a beam current of 25 mA (Fig. 7), there is hardly any change in going from 2000 to 2400 V. The perveance curve shown in Fig. 10 indicates the deflecting operating point must lie far enough to the right of the limiting perveance lines to be in the regime when the accel drain curve has reached its minimum value. Thus, the total voltage must be raised as the beam current level increases to maintain low drains when the beam is deflected. This means the deflection sensitivity necessarily will decrease as the beam current level is increased.

TABLE X

Summary of Different Ion Optical Geometries

Configuration	Screen Hole Size (cm)	Screen Hole Shape	Nominal Screen Open Area (%)	Grid Spacing (cm)	TV Optics Aperture (cm)	I_{ACC} $V_T = 2000V$ (mA)	I_+ = 25 mA Minimum V_{Tot} $I_{ACC} = 0.2$ mA (V)	% Increase in I_{ACC} 140 Def
1	0.394	Round	55	0.119	0.342	0.11	1750	
2	Square*	Square type	55	0.119	0.342	0.12	1740	
3	Square*	Square type	55	0.076	0.342	0.10	1580	
4	0.317	Round	36	0.119	0.342	0.22	2040	
5	0.317	Round	36	0.076	0.266	0.10	1500	~0

* This aperture has the same nominal area (12.2 mm²)

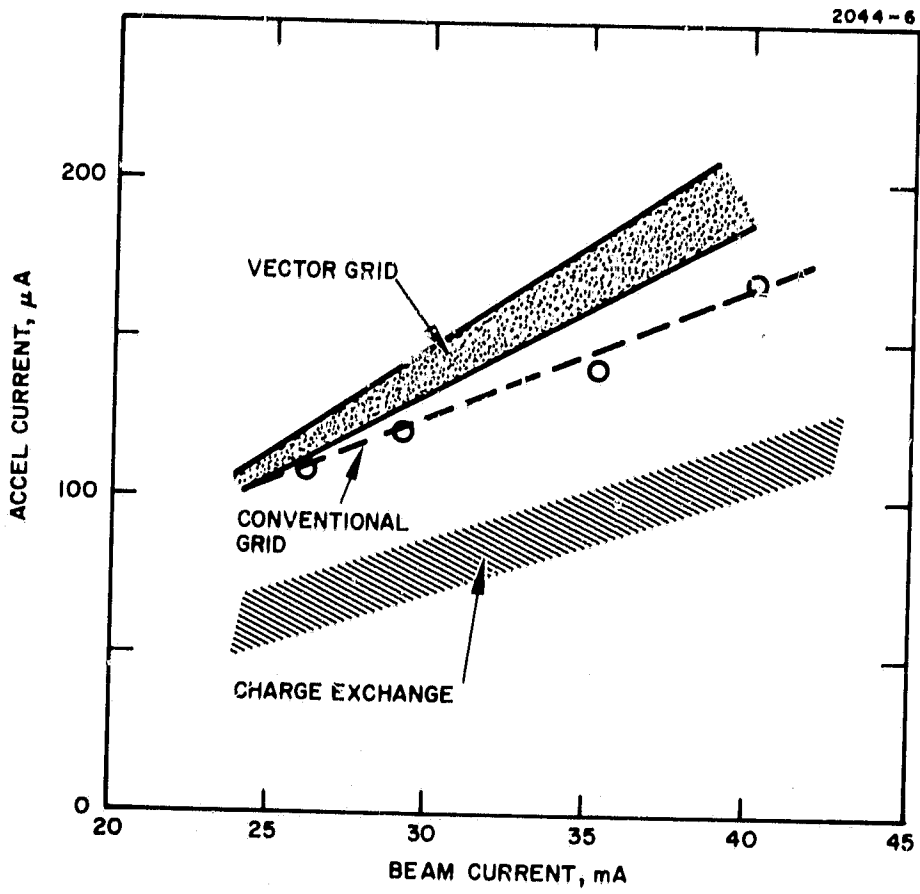


Fig. 6. Measured Undeflected Accel Currents as a Function of Beam Current and Calculated Charge Exchange Currents.

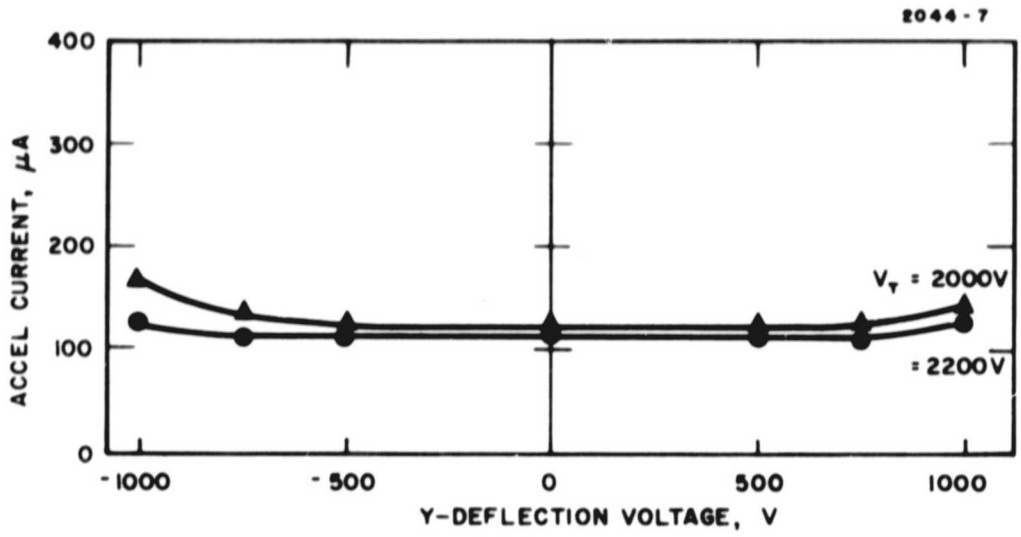


Fig. 7. Accelerator Current Versus Deflection Voltage
 $I = 25 \text{ mA}$.

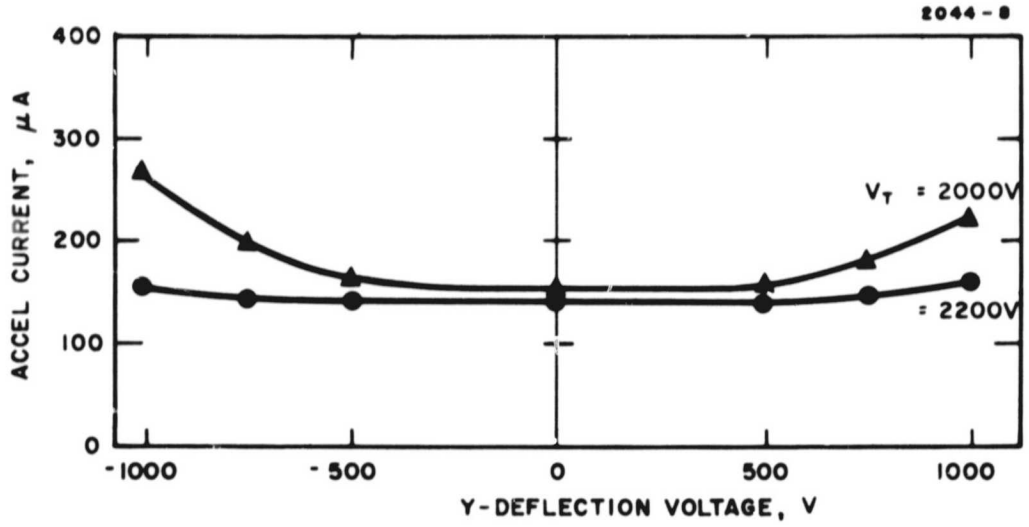


Fig. 8. Accelerator Current Versus Deflection Voltage
 $I = 30 \text{ mA}$.

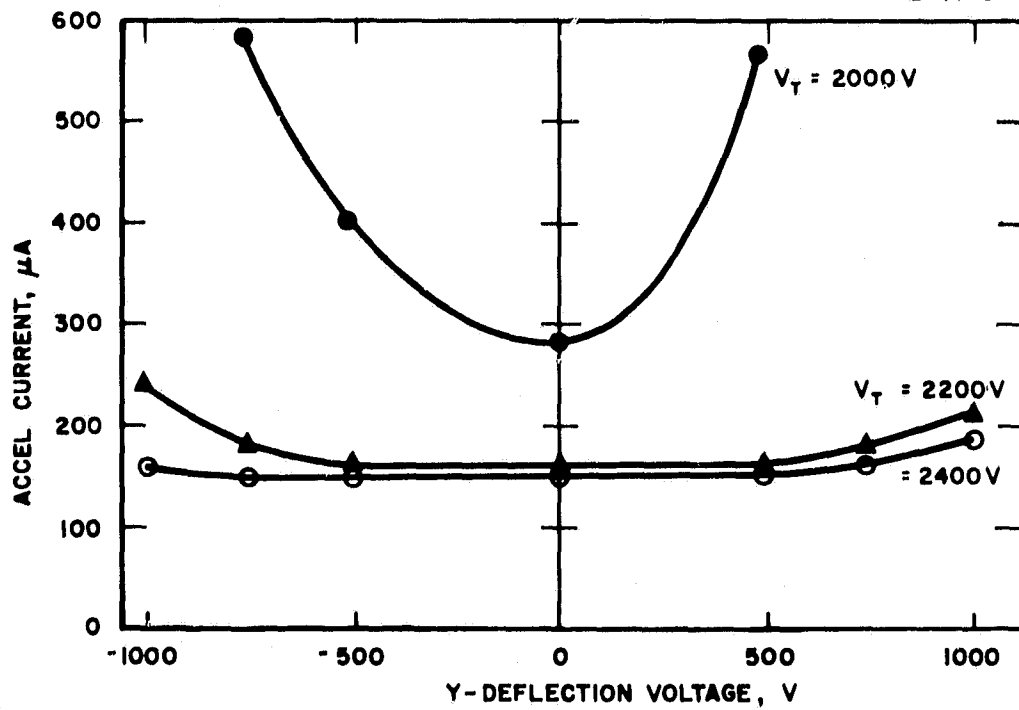


Fig. 9. Accelerator Current Versus Deflection Voltage
 $I = 35\text{ mA}$.

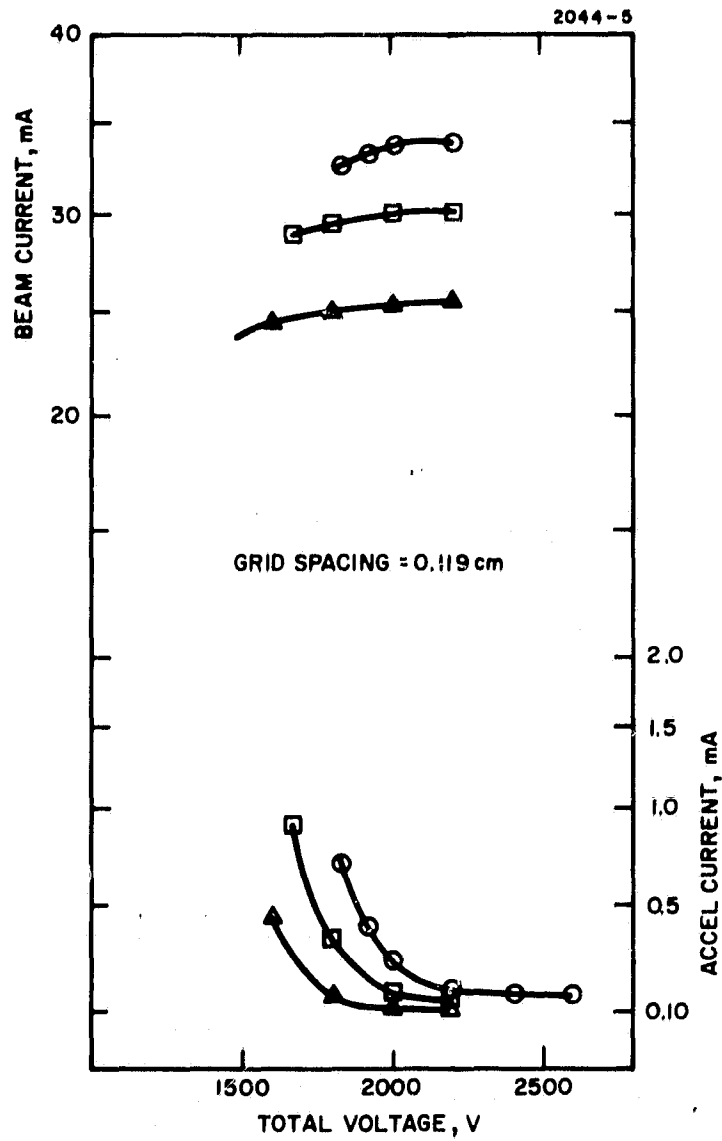


Fig. 10. Perveance Curve.

A comparative summary of the different optics tested is exhibited in Table X.

This data shows the following:

1. Comparing configurations 1 and 2, which have the same grid spacing, there is no apparent advantage in going from the round- to square-type screen aperture.
2. Comparing configurations 2 and 3 (or 4 and 5), the 0.076-cm grid spacing is clearly superior to the 0.119-cm grid spacing. Measurements of the actual beamlet size using thin foil (see the appendix) showed that the closer spacing was producing a smaller beamlet size.
3. Comparing configurations 4 and 5, it is obvious that the 0.317-dia screen hole should not be used with an accel aperture larger than the screen hole.
4. Since configuration 5 has the lowest drain currents and uses the thick accel strips (0.05 cm versus 0.012 cm) that should result in a longer life, it was chosen as the final design. An extensive performance map of this final design is described in the following subsection.

2. Performance Map

This section contains a summary of the special report submitted following the rather extensive performance map of the final 5-cm Thrust Vector System fabricated under this contract.

a. Introduction

The system is comprised of a SIT-5 thruster and thrust vector optics system developed under the present contract (NASA 3-15385). The thruster tests include perveance curves, thruster performance, beam profiles, and beam deflections for beam currents of 20, 25, 30, and 34 mA, respectively. The thruster was operated for approximately 150 hours with no observable changes in deflection system sensitivity or thruster performance. The purpose of these tests was

to demonstrate that the deflection optics lifetime has been maximized by reducing the ion impingement without sacrificing the deflection sensitivity of previous designs.

b. Thruster and Test Facilities

The SIT-5 thruster that was integrated with the thrust vector optics for these tests was developed under Contract NASA 3-15483. The dimensions of the dual grid electrostatic system are shown in Table XI.

TABLE XI
Dimensions of Dual Grid Electrostatic System

Number of holes	89	
Screen aperture diameter	0.318 cm	0.125 in.
Center-to-center spacing	0.444 cm	0.175 in.
Accel aperture diameter	0.267 cm	0.105 in.
Screen thickness	0.051 cm	0.020 in.
Accel thickness	0.254 cm	0.100 in.
Screen-accel spacing	0.076 cm	0.030 in.
Pole piece	H (see Fig. 3)	

T808

Figure 11 gives the dimensions on an individual hole. Figure 1 is a photograph of the optics system prior to mounting on the thruster.

The test apparatus consists of a 1.5-m diameter by 4.6-m long vacuum chamber equipped with a cylindrical cryoliner and water-cooled beam collector. The thruster is mounted from the end bell so it is completely exposed to the cryoliner, and the beam is not apertured by any port or valve. A conventional electronic test setup was used with

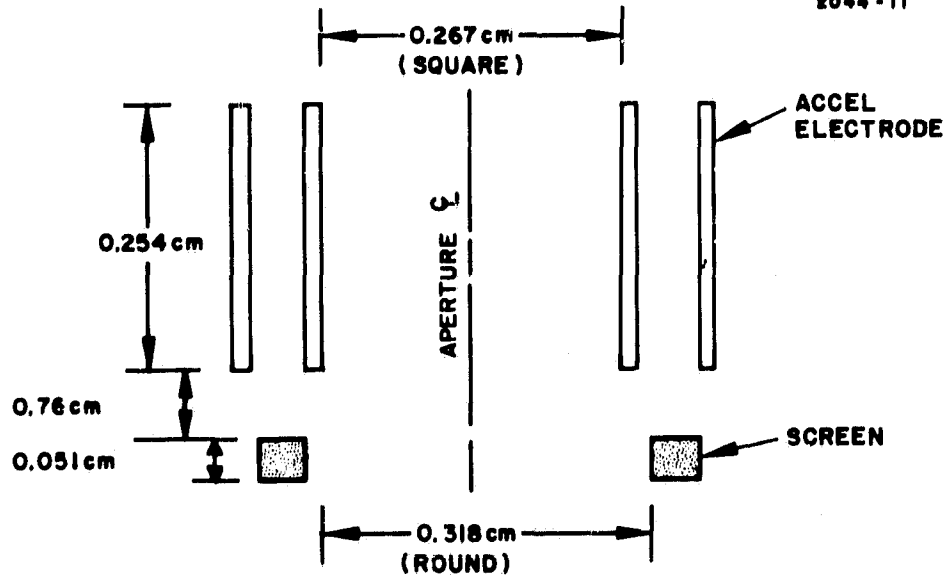


Fig. 11. Aperture Dimensions of Dual Grid Electrostatic Deflection System.

the common point of the positive and negative high voltage supplies and the neutralizer coupled to ground through an SCR to assure a neutralizer emission equal to the beam current without permitting this common point to float to high voltage in the event of a neutralizer failure.

The deflection supply was especially constructed for this type of optics system. It consists of four supplies, ganged in pairs to provide differential voltages in both the x and y directions. The circuit and metering are illustrated in Fig. 12. A current sensing circuit is included in each output to provide overload protection by tripping off the supply.

A rather sophisticated beam probe was used on this program. The 65-cm long probe contains 35 individual faraday cups behind 0.16-cm diameter apertures. (In this test, only 13 cups were used to reduce the data collection time.) The probe carrier runs on two tracks that allow it to be positioned in the z direction (parallel to chamber centerline) and the x direction (horizontal and perpendicular to the chamber centerline); positioning is accomplished by two pulse-driven stepper motors actuated from outside the tank. Thus, the beam intensity may be sampled within the volume downstream of the thruster ranging from $x = \pm 33.4$ cm, $y = \pm 30.5$ cm, and $z = 3.2$ to 64.8 cm from the accelerator electrode.

Circuitry was provided to automatically step the probe carrier in the x and z directions. The magnitude of the beam current samples collected in the probe cups was automatically recorded on punched tape, which could be fed directly into the computer for analysis. In operation, a typical scan consisted of setting the probe carriage at the desired z distance and then scanning each of 13 faraday cups at 13 preselected, equally spaced positions in the x direction. Such a scan takes approximately 6-1/2 min to perform.

The data was analysed by using the computer to fit a three-dimensional surface to the beam intensity measurements taken in a particular surface to the beam intensity measurements taken in a particular plane. The computer calculates the position of the centroid of the volume defined by this surface, the magnitude of the total current

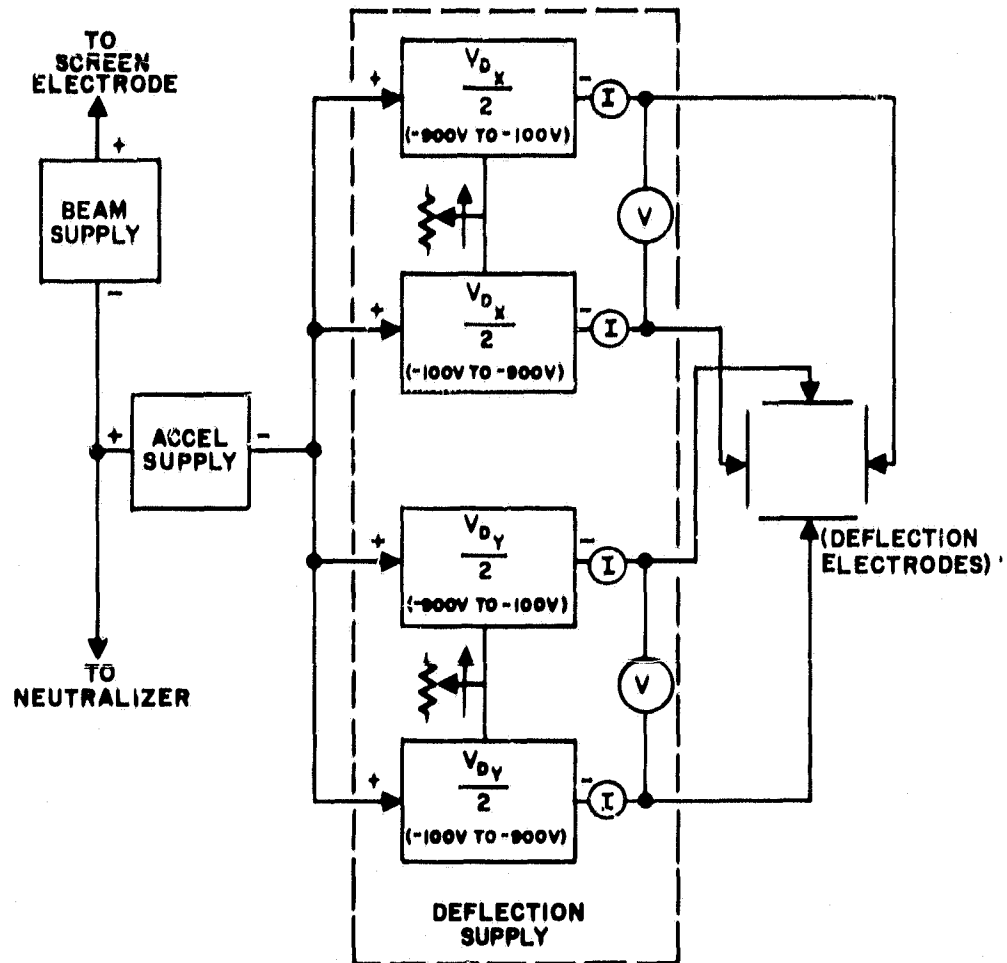


Fig. 12. Functional Diagram of Deflection Power Conditioning.

represented by the surface, and the location of the curves of equal current intensity over the surface. These latter contours can be plotted automatically by the computer, using a Calcomp plotter if desired. This was done periodically to check the beam shape, but was too time-consuming (~20 min/plot) to do each of the scans taken during the testing.

c. Test Procedure

Deflection data and thruster performance information was obtained for beam currents of 20, 25, 30, and 34 mA, respectively. Selected beam and accel voltages are described in the results in the following pages. The thruster was operated overnight, between deflection experiments, to obtain mass flow data. All data were taken with chamber pressure in the 10^{-7} to 10^{-8} Torr range.

d. Perveance Curves

Perveance curves were taken for the SIT-5 thruster at four different beam levels. When $V_+ = 1600$ V and $V_- = -800$ V, the beam values were nominally 20, 25, 30, and 34 mA, respectively. Figure 13 shows the perveance data along the corresponding accel current. It can be seen that this system adequately handles a beam current of 34 mA at a total voltage of 2000 V, and a beam of 20 mA at 1350 V. Note that for the 25 mA planned operating current for this thruster, the accel current starts to increase when the total voltage drops to 1650 V. This is 750 V below the 2400 V nominal total voltage. A plot of beam current versus accel drains ($V_+ = 1600$ V; $V_- = -800$ V) shows a linear relationship in Fig. 14.

e. Thruster Performance

The performance values in Table XII were obtained at the beam current levels of 20, 25, 30, and 34 mA. Mass utilization values were obtained from runs of 20 hours or greater. The SIT-5 thruster discharge performance is shown in Fig. 15 for four propellant flow rates. These correspond to ion beam currents of 20, 25, 30, and 34 mA.

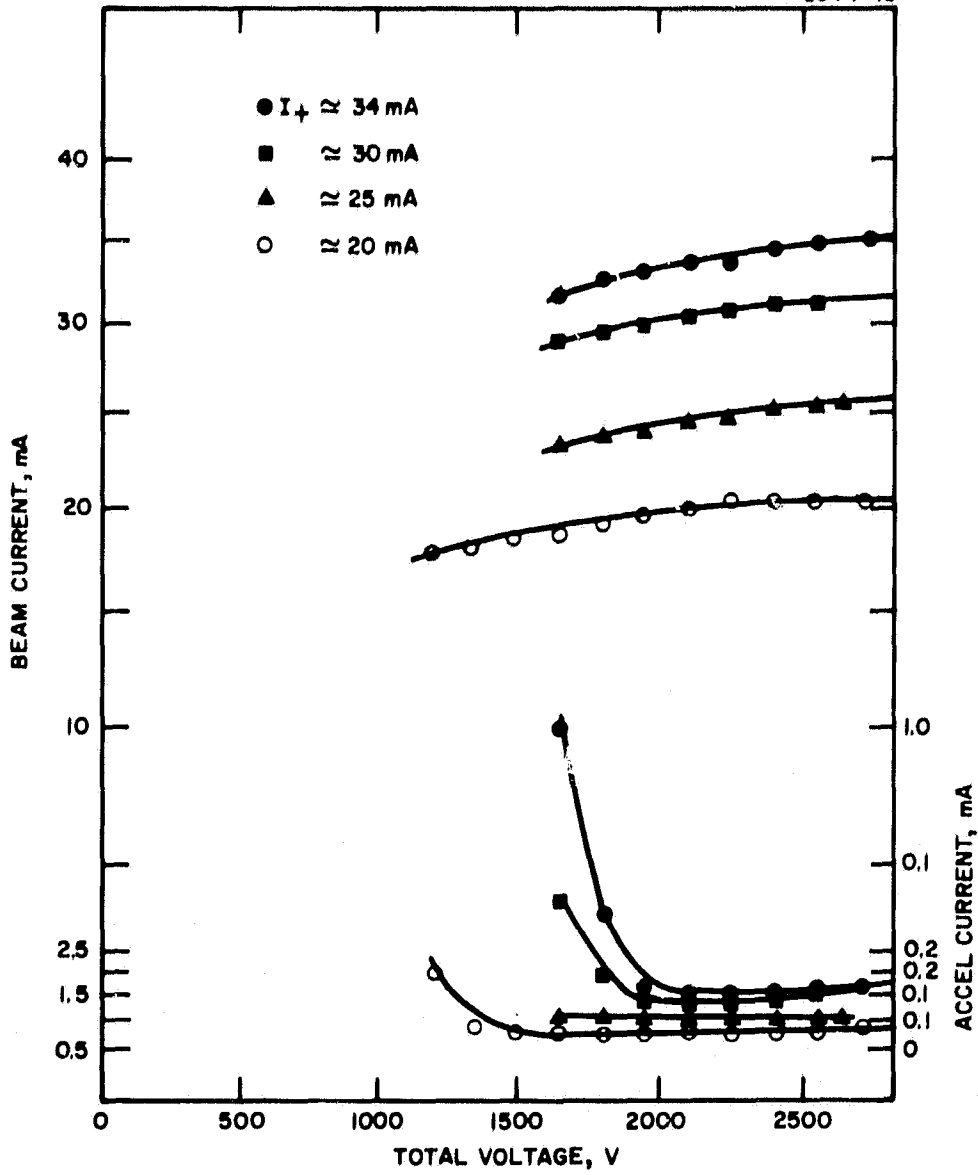


Fig. 13. Measured Perveance Curves for 0.125 in. Diameter Screen Holes, 0.105 Accel Apertures, 0.030 in. Grid Spacing.

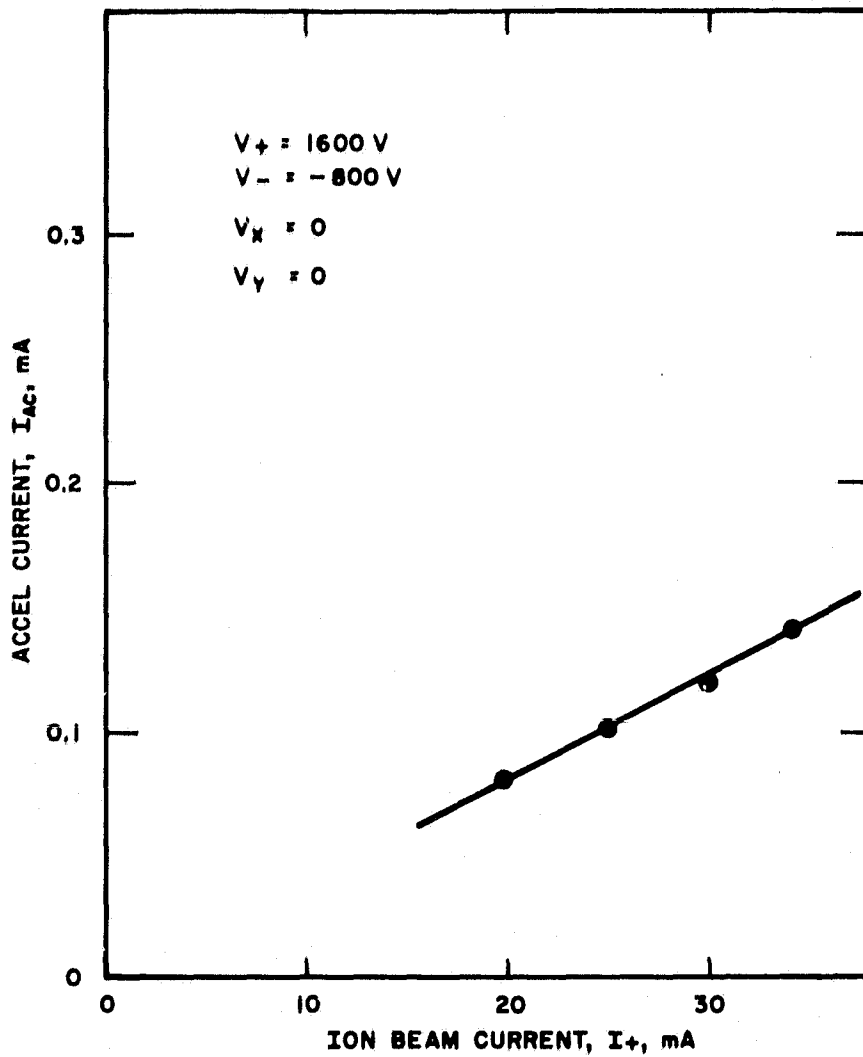


Fig. 14. Accel Current Versus Ion Beam Current.

TABLE XII

SIT-5 Thruster Performance with
Thrust Vector Optics

Beam Voltage, V_t , V	1600	1200	1200	1600
Beam Current, I_B , mA	20	25.5	30.1	34
Accel Voltage, V_a , V	-800	-1160	-1160	-800
Discharge Chamber Voltage, V_D , V	45	45	45	45
Discharge Chamber Current, I_D , mA	200	300	380	435
Neutralizer Coupling Voltage, V_C , V	12	25	28	40
Neutralizer Coupling Current, I_C , mA	20.5	25.5	30.6	34.5
Main Keeper Voltage, V_{MK} , V	20	16.5	16	16
Main Keeper Current, I_{MK} , mA	370	370	370	370
Neutralizer Keeper Voltage, V_{NK} , V	21	22	23	20
Neutralizer Keeper Current, I_{NK} , mA	360	360	400	450
Discharge Energy/Ion, V_{DISCH} Ω eV/Ion	450	529	568	575
Discharge Mass Utilization, N_m , %	68	69	65	72
Neutralizer Flow, I_{NHg} , mA	2.1	3.6	3.4	4.2

T809

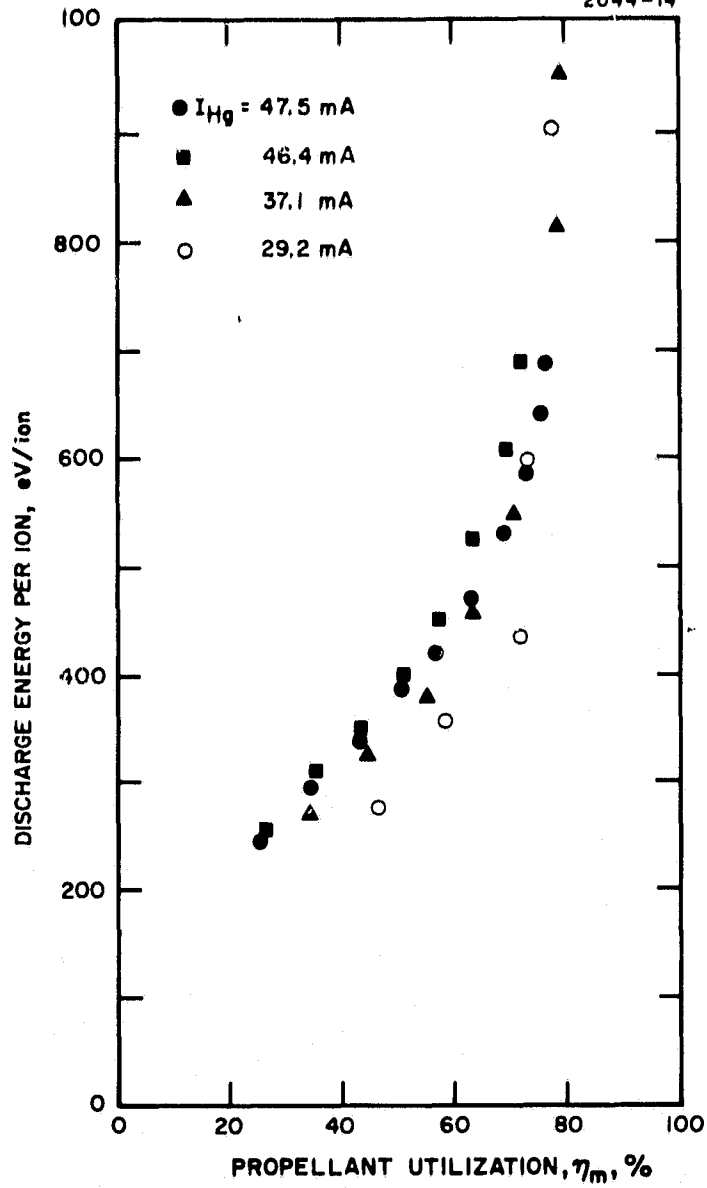


Fig. 15. Discharge Energy per Ion Versus Propellant Utilization.

f. Beam Profiles and Deflection Results

The beam profiles and deflections were taken for 20, 25, 30, and 34 mA beams with the beam scanner. Various beam and accel voltages were used to demonstrate their effect on the beam deflection. Table XIII contains the data that was taken. The significance of the positive and negative signs of the V_X and V_Y deflection voltages was merely the sign convention for the center zero voltmeter used to measure the deflection voltage.

The most detailed deflection curves were obtained for $V_+ = 1600$ V, $V_- = -800$ V, at the four beam currents mentioned earlier. The results of the X deflection are shown in Figs. 16 through 19. The deflections are similar. The sensitivity obtained from these figures is shown in Table XIV as obtained from the slope of the curves. Generally speaking, a slightly larger deflection angle is obtained for larger beam currents. This is because the broader beams experience a larger deflection force. As illustrated, the Y deflection sensitivity is slightly higher than the X deflection sensitivity. Previous experiments, with the same notch orientation as these experiments in which the notches in the Y strips (which deflect the beam in the X direction) were oriented downstream, had a higher deflection sensitivity in the X direction. Evidently the downstream sputter shields (which were not present in the previous experiments) have increased the Y sensitivity enough to reverse the previously observed behavior.

Tables XV and XVI show the deflection angle for various voltages at limiting beam currents of 20, and 34 mA, respectively. These tables verify that the sensitivity is less for the more energetic beams. Table XVII shows the deflection angle for $V_+ = 1400$ V, $V_- = -700$ and $V_+ = 1800$ V, $V_- = -900$ V, at various beam levels.

A final check on the axis of the thruster with respect to the normal of the scanning collector plane was made by obtaining non-deflection readings at three distances from the thruster. These results showed that the thruster was pointed upwards approximately 4° .

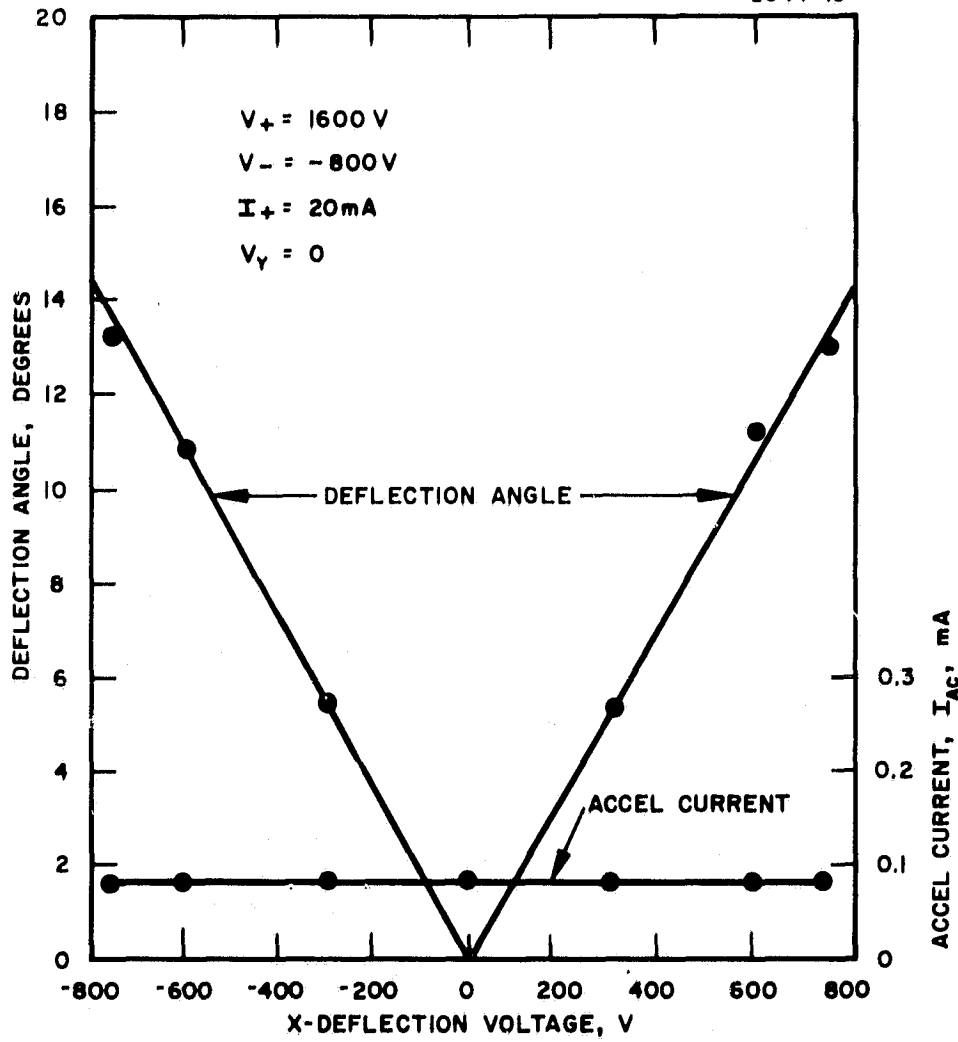


Fig. 16. Deflection Angle Versus X-Deflection Voltage ($I_t = 20 \text{ mA}$).

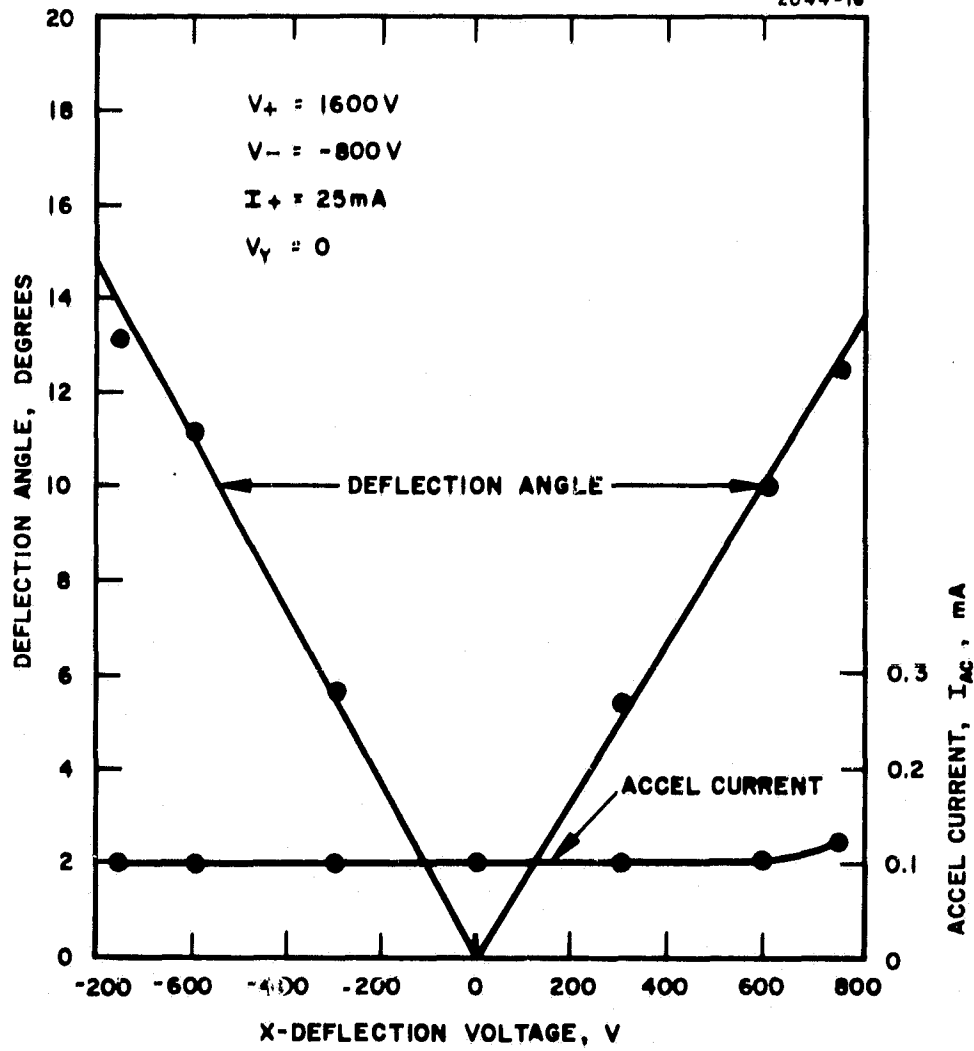


Fig. 17. Deflection Angle Versus X-Deflection Voltages ($I_t = 25$ mA).

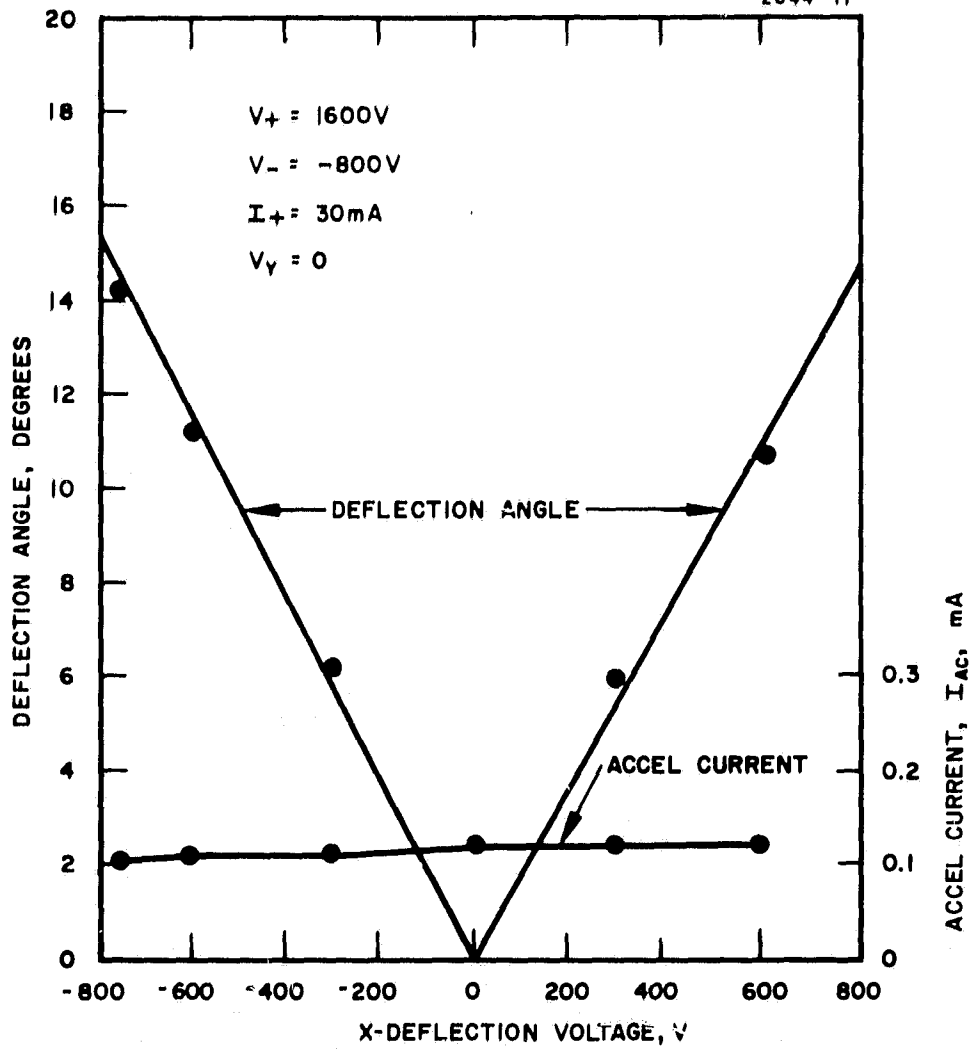


Fig. 18. Deflection Angle Versus X-Deflection Voltage ($I_t = 30 \text{ mA}$).

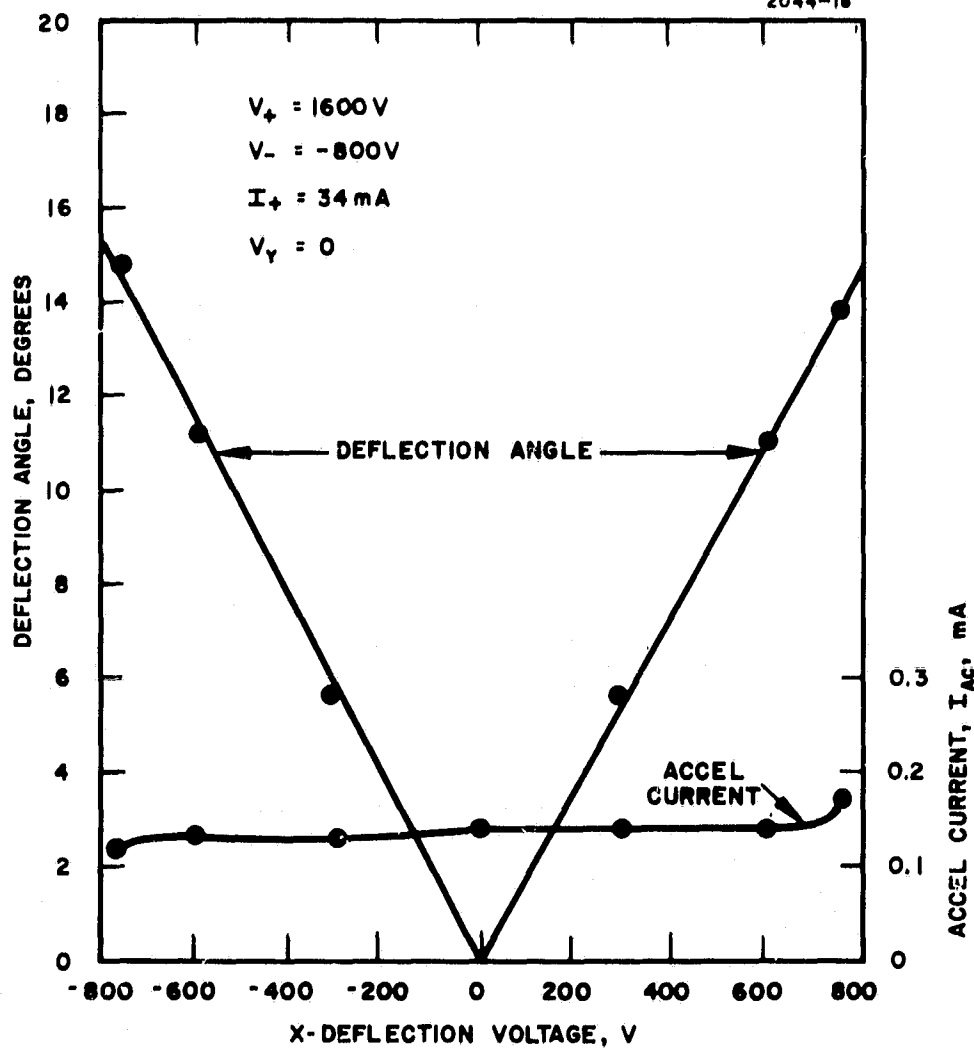


Fig. 19. Deflection Angle Versus X-Deflection Voltage ($I_t = 34$ mA).

TABLE XIII

Beam Profile and Deflection Data

I_B	$V_+ = 1400$ $V_- = 700$	$V_+ = 1600$ $V_- = 800$	$V_+ = 1800$ $V_- = 900$	$V_X = 0$ $V_Y = 0$	$V_X = \pm 300$ ± 600 ± 750 $V_Y = 0$	$V_Y = \pm 300$ ± 600 ± 750 $V_X = 0$	$V_X = \pm 600$ $V_Y = 0$	$V_Y = \pm 600$ $V_X = 0$
20 mA	X			X			X	X
20 mA		X		X	X	X	X	X
20 mA			X	X			X	X
25 mA	X			X			X	X
25 mA		X		X	X	X	X	X
25 mA			X	X			X	X
30 mA	X			X			X	X
30 mA		X		X	X	X	X	X
30 mA			X	X			X	X
34 mA	(X)							
34 mA		X		X			X	X
34 mA			X	X			X	X

(X) — No data; accel current too high.

TABLE XIV

Deflection Sensitivity for $V_+ = 1600$ V, $V_- = -800$ V

V_+ V	V_- V	I_+ mA	V_X V	V_Y V	$\frac{d\theta}{dV_x}$ degree/V	$\frac{d\theta}{dV_y}$ degree/V
1600	-800	20	+	0	0.0179	
1600	-800	25	+	0	0.0170	
1600	-800	30	+	0	0.0184	
1600	-800	34	+	0	0.0186	
1600	-800	20	-	0	0.0179	
1600	-800	25	-	0	0.0184	
1600	-800	30	-	0	0.0192	
1600	-800	34	-	0	0.0191	
1600	-800	20	0	+		0.0181
1600	-800	25	0	+		0.0188
1600	-800	30	0	+		0.0200
1600	-800	34	0	+		0.0224
1600	-800	20	0	-		0.0181
1600	-800	25	0	-		0.0224
1600	-800	30	0	-		
1600	-800	34	0	-		0.0193

T811

TABLE XV

Deflection Data for a 20 mA
Beam and Various Total Voltages

V_+ V	V_- -V	V_T V	I_+ mA	I_{AC} mA	V_X V	V_Y V	θ_X degrees	θ_Y degrees
1400	700	2100	20	0.075	600	0	12.3	0
1600	800	2400	20	0.08	600	0	11.3	0
1800	900	2700	20	0.08	500	0	8.4	0
1400	700	2100	20	0.07	-600	0	-12.2	0
1600	800	2400	20	0.08	-600	0	-10.9	0
1800	900	2700	20	0.08	-600	0	-9.4	0
1400	700	2100	20	0.07	0	600	0	14.6
1600	800	2400	20	0.07	0	600	0	12.4
1800	900	2700	20	0.075	0	600	0	10.9
1400	700	2100	20	0.075	0	-600	0	-12.4
1600	800	2400	20	0.07	0	-600	0	-11.0
1800	900	2700	20	0.07	0	-600	0	-9.9

T812

TABLE XVI

Deflection Data for a 34 mA
Beam and Various Total Voltages

V_+ V	V_- -V	V_T V	I_+ mA	I_{AC} mA	V_X V	V_Y V	θ_X degrees	θ_Y degrees
1600	800	2400	34	0.14	600	0	11.0	0
1800	900	2700	34	0.13	600	0	10.0	0
1600	800	2400	34	0.13	-600	0	-11.1	0
1800	900	2700	34	0.125	-600	0	- 9.7	0
1600	800	2400	34	0.13	0	600		
1800	900	2700	34	0.125	0	600	0	12.4
1600	800	2400	34	0.13	0	-600	0	-11.4
1800	900	2700	34	0.14	0	-600	0	- 9.9

T813

TABLE XVII

Deflection Data for Similar Voltages
and Various Beam Currents

V_+ V	V_- -V	V_T V	I_+ mA	I_{AC} mA	V_X V	V_Y V	θ_X degrees	θ_Y degrees
1400	700	2100	20	0.075	600	0	12.3	0
1400	700	2100	25	0.11	600	0		
1400	700	2100	30	0.13	600	0	12.9	0
1400	700	2100	20	0.07	-600	0	-12.2	0
1400	700	2100	25	0.09	-600	0	-13.8	0
1400	700	2100	30	0.11	-600	0	-13.1	0
1400	700	2100	20	0.07	0	600	0	14.6
1400	700	2100	25	0.09	0	600	0	12.9
1400	700	2100	30	0.12	0	600	0	13.8
1400	700	2100	20	0.075	0	-600	0	-12.4
1400	700	2100	25	0.10	0	-600	0	-11.0
1400	700	2100	30	0.11	0	-600		

T814

This would give an error of less than $\pm 0.5^\circ$ to the deflection data. Based on this and an estimate of other possible errors, the accuracy of the measured deflection angles can be said to be better than $\pm 1^\circ$.

g. Conclusion

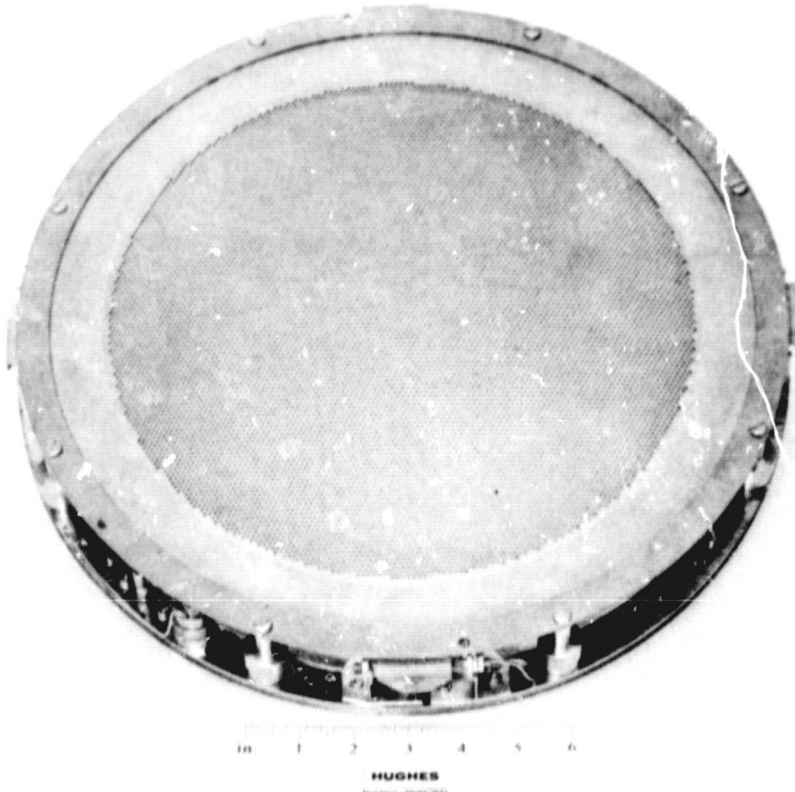
The results of the deflection studies show that for the design operating point (i. e., $V_+ = 1600$, $V_- = -800$, and $I_+ = 25$ mA) deflection angles of $\pm 10^\circ$ can be obtained readily with deflection voltages of ± 600 V or less. The accel currents are quite low (0.10 mA) and promote long lifetimes. These tests also provide useful deflection data for off-design operating points.

D. CONCLUSION

1. 5-cm Electrostatic Thrust Vector System

A structurally sound, high-response thrust vectoring system has been constructed for the 5-cm SIT-5 thruster system. The system easily produces $\pm 10^\circ$ deflection to any azimuth without reducing the system lifetime. Life tests approaching 10^4 hours duration are currently underway at the NASA Lewis Research Center. The only detriment of the system is an apparent 5 to 10% degradation in thruster mass utilization as compared to performance measured with a conventional two-electrode system. Tests are currently underway to optimize the discharge chamber for the vectorable electrode geometry to eliminate this performance penalty.

M9041



30cm THRUST VECTORING SYSTEM

SECTION III

PART II - 30-cm SYSTEM

A. PROGRAM OUTLINE

The initial task under this phase of the program was to fabricate and test a movable grid, 30-cm thrust vectoring system patterned after a similar 5-cm system that had been developed previously and successfully tested under Contract NAS 3-14058. A large area array of faraday cups was constructed to facilitate accurate analysis of the ion beam shape and profile in the 9-ft space simulation facility. The test results demonstrated that the moving screen concept worked satisfactorily in the 30-cm size, but that an improved grid support and actuator system were required for mechanical stability.

A survey of other possible actuators was conducted and submitted to NASA LeRC with proposed structural design modifications to improve the integrity under launch conditions. This design was approved and the request was made that the final system incorporate dished electrodes to eliminate the need for a central interelectrode support.

Two sets of electrodes were built to this design and satisfactorily tested to experimentally demonstrate the ability to vector a broad 2-A ion beam with an ion optical system of the same apertured configuration, perveance, and general mechanical structure as currently used in optimization programs and life tests at NASA LeRC and at HRL.^{4,5} While no vibration tests were made, the much stiffer mounting structure and the dished electrodes used in the latest design appear to have a mechanical integrity equal to the rest of the thruster structure. The grids were delivered to LeRC for further testing.

B. MECHANICAL DESIGN - 30-cm SYSTEM

Design Details - 30-cm Deliverable Hardware

The initial 30-cm vectorable grid system was fabricated and tested on the GFE thruster designed and fabricated under Contract NAS 3-14140.

The entire optics system, including the grid supporting hardware, is a complete bench subassembly and is demountable from the thruster. The screen and accelerator electrodes are supported from a lightweight annular ring, which provides a stable mounting base for the optics and a convenient interface to the mounting brackets on the thruster outer housing.

The screen electrode is supported by six helical springs attached to the screen electrode mounting brackets and is also held by support wires at the periphery and by a center support. The helical springs, when heated by passing current through them, serve as the motion generating device. The flexible columns provide the proper axial spacing while allowing flexibility in the transverse direction with a minimum of resisting force. The grid center support design consists of a 0.05-cm diameter x 2.8-cm long molybdenum wire with a flange electron beam welded to the upstream end. A screw is beam welded to the downstream end, which attaches to the accel grid by an insulated cap. The cap is the only portion of the center support downstream of the accelerator grid. An outer tube is brazed to the screen grid and is machined on the upstream end to accommodate the flange, insulators, and retaining screw.

The calibration of the screen electrode motion versus power was accomplished (in vacuum) by mounting two linear differential transformers on the X and Y axis of the thrust vectoring optics assembly. The output of these transducers was displayed with a digital display giving a direct readout of the X and Y motion to a resolution of 0.0001 in. Since the spring orientations were as shown

in Fig. 20, different groupings of springs were used for the X and Y directions. Thus, for the Y direction, either spring numbers 6 and 5, or 2 and 3 were heated, while for the X direction, spring numbers 1, 2 and 6, or 3, 4 and 5 were heated. Figure 20 shows the resulting measured screen translation as a function of the total input power for various spring orientations. This figure shows that using either two or three adjacent springs, depending on the direction desired, a screen movement of 0.2 mm can be obtained with about 0.8 W total heating power. From the recent results of Lathem,⁶ this should result in a beam deflection angle of approximately 10° . During these tests, the maximum translation obtained was about 0.35 mm, which corresponds to a deflection angle of approximately 17° .

This grid system demonstrated the applicability of vectoring a large beam by the moving screen technique; however, it indicated that structural modifications were required for improvement of the system mechanical and thermal stability to achieve reliable operation over the full power range and during launch conditions. Several alternate designs were analyzed, and the most promising was implemented into test hardware. Basically, this design consists of a reservoir filled with liquid mercury which is coupled to actuator bellows that elongate when the reservoir is heated. This device is shown schematically in Fig. 21. The fluid (liquid mercury) fills the region between bellows A and the outer container, the connecting tube, and bellows B. As the system heats up to the nominal operating temperature, the mercury expands and compresses bellows A (which has a lower spring rate than bellows B) until it is constrained by the stop screw. The stop screw is adjustable to compensate for variable ambient temperatures.

The completed system is shown in Fig. 22. Work on related 30-cm programs had progressed so it was possible to incorporate hydrostatically formed dished grids for the final deliverable hardware, thus eliminating the need for a central interelectrode support. In this design, a single reservoir is used to drive two bellows at diametrically opposite points, as shown schematically in Fig. 23.

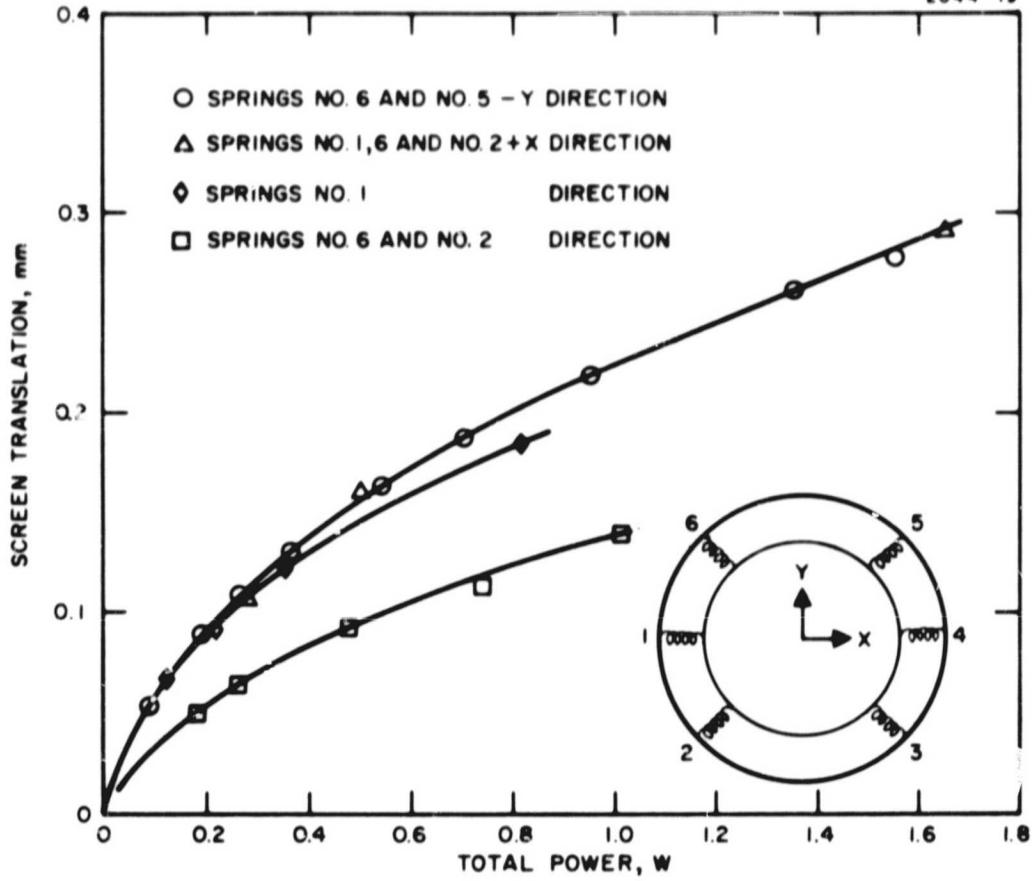


Fig. 20. Screen Translation as Function of Total Input Power for Different Spring Orientations.

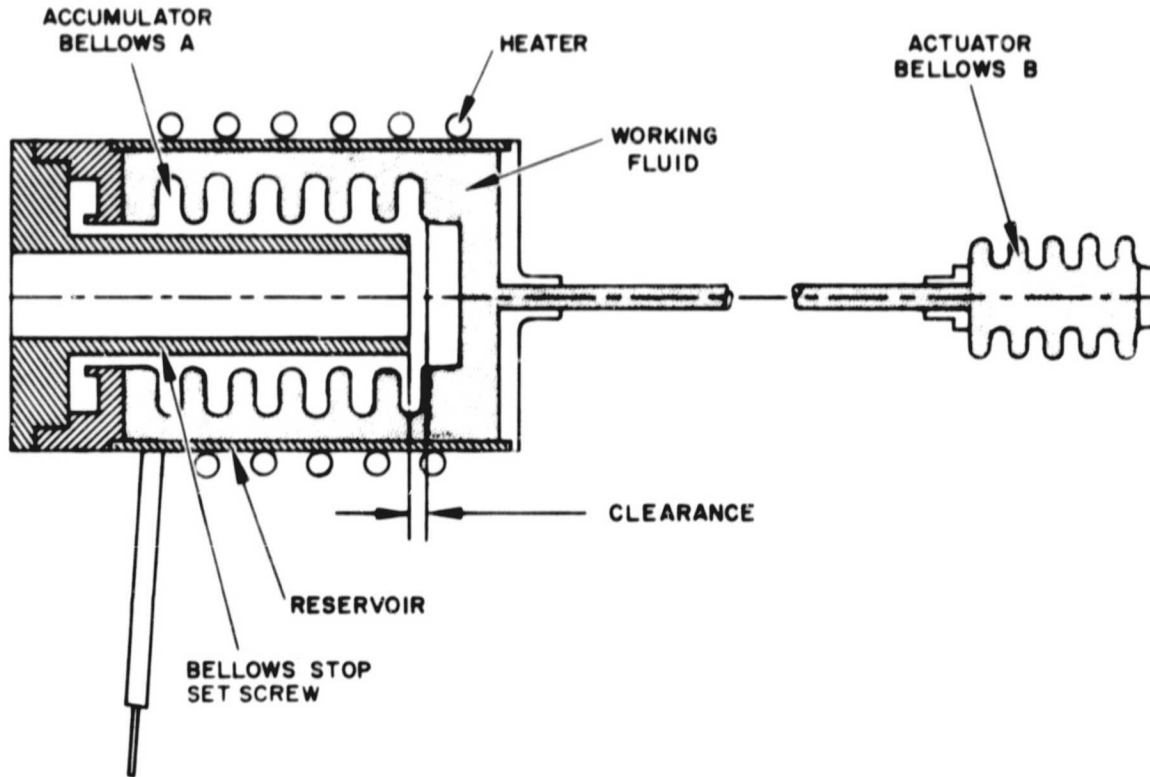
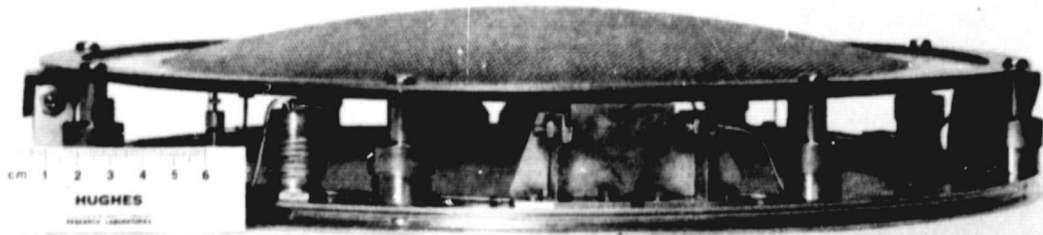


Fig. 21. Schematic of Expanding Fluid Motion Generator.

M9042



M9040

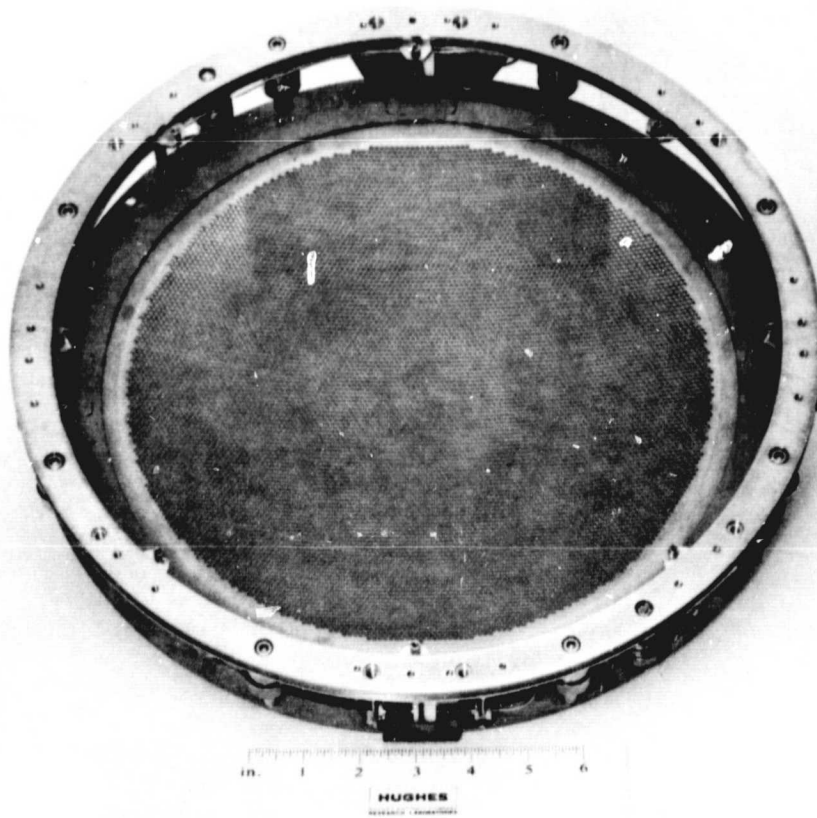


Fig. 22. 30-cm Thrust Vectoring System.

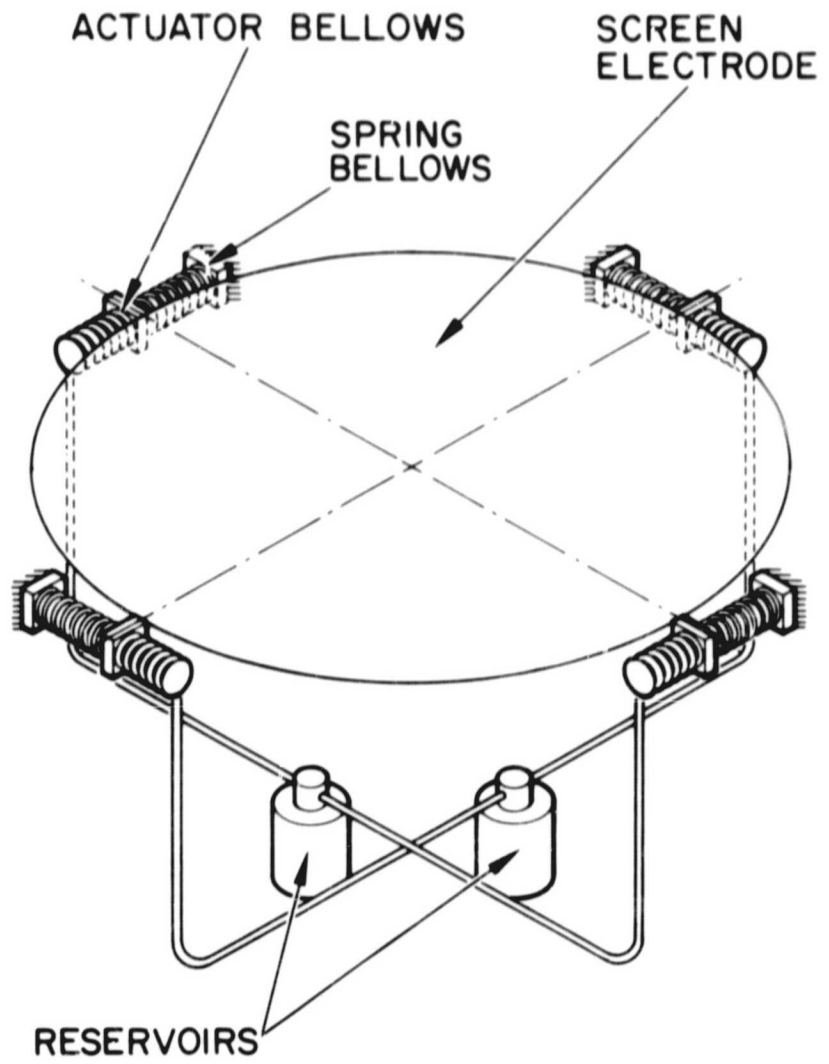


Fig. 23. Thrust Vectoring Actuator Concept.

If only single bellows were used on each axis, the screen electrode would rotate due to the lateral instability on compression springs (bellows).

C. SYSTEM PERFORMANCE EVALUATION

All thruster tests were made on a 30-cm thruster of the type developed under Contract NAS3-14140. The tests were run in the 3-m diameter space simulation facility, which had been equipped with an array of 177 small faraday cups spaced 15-cm apart. The beam current entering these cups was sequentially monitored with a digital voltmeter to provide a data format similar to that described in Section II-C for the 5-cm tests. The data was recorded on punched tape and analyzed by computer to provide beam centroid location and an integrated value for the total collected ion beam current. If desired, the beam contours at each of the 10% intensity levels can be presented graphically at the recorder output of the computer. The lateral motion of the electrodes was measured with a linear differential transformer.

1. Test of the Prototype System (SN 50)

As described above, the prototype system employed flat grids with a single central interelectrode support. The screen was actuated by controlling the temperature of the support springs, which provided its mechanical lateral support.

The measured beam deflection is shown in Fig. 24.

During the tests, several observations were made, as follows:

- a. The beam deflection angle was $0.7^\circ/0.001$ in. of electrode motion that is in agreement with the design predictions.
- b. Thruster performance with the vectorable optics was equivalent to that with the original non-vectorable grids, as had been expected.

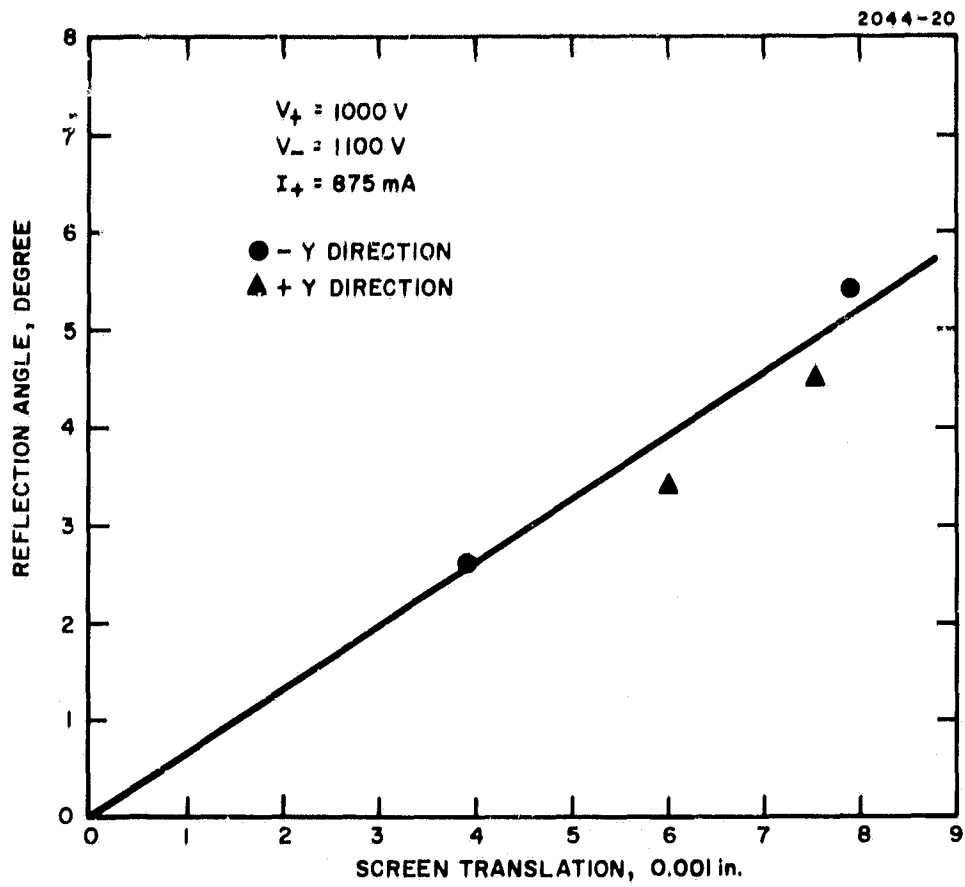


Fig. 24. Measured Beam Deflection as Function of Screen Translation.

- c. Although several attempts were made to adjust the electrode spacings, the maximum stable beam current that could be extracted was ~1.0 A. Above this value, interelectrode shorting and arcing occurred. This problem also arose in non-vectorable electrode systems fabricated at this time and it has been traced recently to the accelerator mounting structure.
- d. The weight of the screen electrode caused observable grid misalignment as the thruster orientation was changed. This indicated that a modified mounting arrangement was required — particularly to withstand launch conditions.
- e. The power required to move the electrode a given amount increased as the ambient thruster temperature increased. This is due to the increased heat loss from the springs as the thruster temperature was raised. At maximum deflection, the spring temperature increased to the point where a permanent mechanical set could take place.

The conclusion to be drawn from these prototype system tests is that the basic concept is good, but that the structural design and the method of moving the screen electrode should be improved. Specifically, the improved design should:

- a. Provide a more positive mount for the screen electrode, particularly with the thruster off, as it would be during launch.
- b. Provide a positive displacement motion generator rather than the present variable force system. With the latter, the electrode motion is a function of the resisting force, thus making it difficult to precalibrate this motion prior to launch.
- c. Eliminate the need for a center support without sacrifice of interelectrode spacing accuracy.
- d. Not be sensitive to the temperature change incurred when the thruster is first turned on or when adjacent thrusters are switched on, thus making the thermal environment around the thruster nonuniform.
- e. Assure that both the screen and accelerator take on the same direction of curvature as they expand due to the temperature gradient from center to edge. Failure to do this was identified as the cause of interelectrode arcing at 1.0-A beam current.

2. Test of Final Delivered System (SN's 503 and 504)

a. Bench Tests

Prior to integration with the thruster, the ion optical systems were thermally tested on the bench to establish the motion generated for a given temperature increment. These results are shown in Fig. 25 and indicate that, as desired, the response is the same for both the X and Y translators. Figure 26 also compares the sensitivity of the two assemblies. Initial data was taken with the actuator set to make no provision for an ambient temperature increase prior to the start of translation. When the stop in the actuator is backed off to permit the accumulator bellows to compensate for an ambient temperature increase, curves with a distinct knee are recorded, as shown in Fig. 25. The knee may occur at a slightly different temperature when the extractor system is on the thruster, because each of the various mercury-containing elements will rise to its own ambient temperature and affect the mercury volume.

b. Thruster Tests

The thruster and vectorable optics were mounted in the 3-m diameter by 6-m long space simulation facility for tests. The multiple-probe array was set at the maximum distance, approximately 4 m downstream of the thruster. With the much broader beam produced by the dished optics, the beam at this location proved to be very flat and the centroid could not be determined with sufficient accuracy to precisely define the thrust vector. The collector was next moved to a location 127 cm downstream, with the much more definitive results reported below. All transverse motions are measured in this plane.

The test data are illustrated graphically in Figs. 26 through 28. Figure 26 shows the inter-relationship of ion beam current (discharge chamber power), actuator temperature, and actuator heater power (actuator heater resistance $\sim 1 \Omega$). The actuator ambient

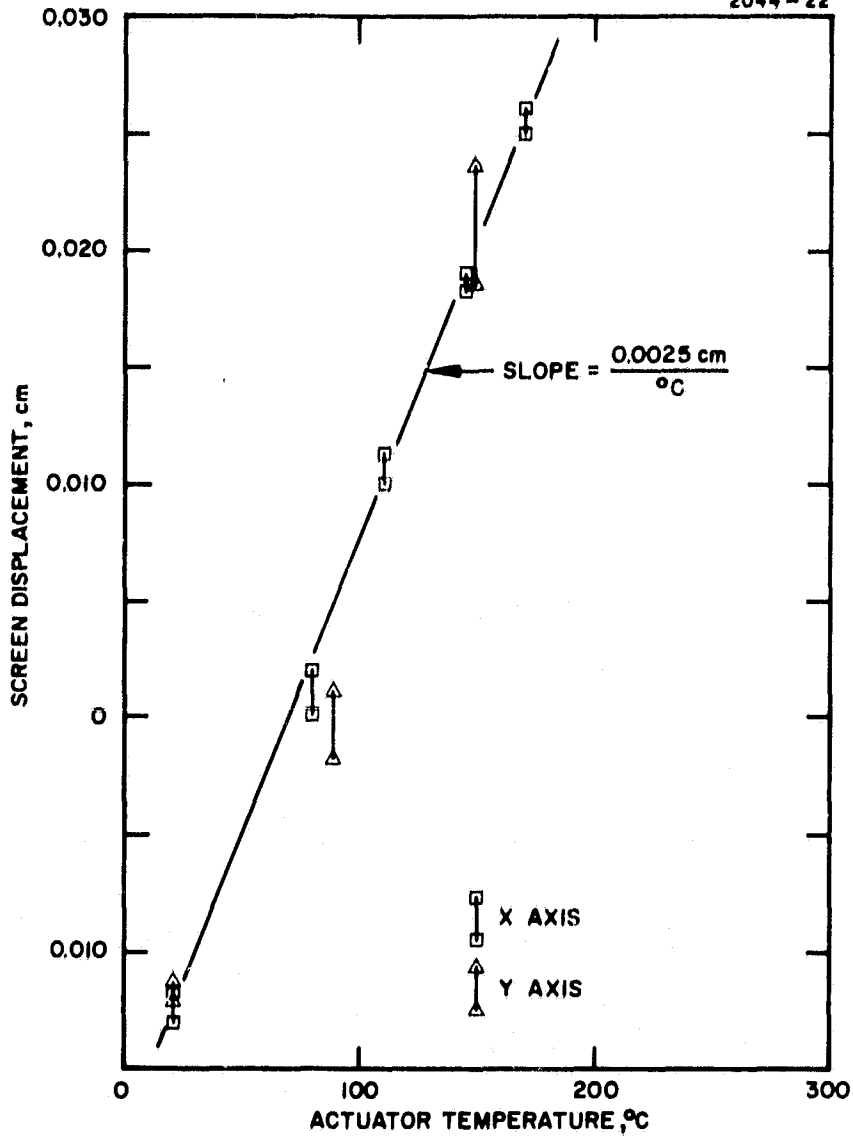


Fig. 25. Ion Optical Systems Thermal Test Results.

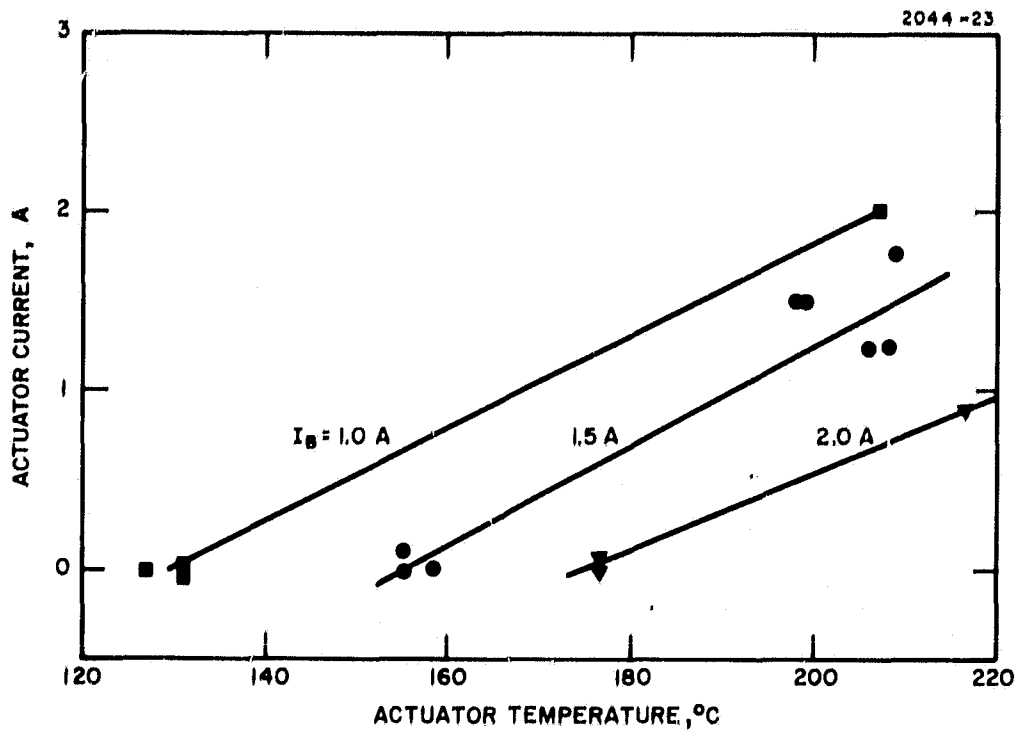


Fig. 26. Relationship Between Ion Beam Current, Actuator Temperature, and Actuator Heater Power.

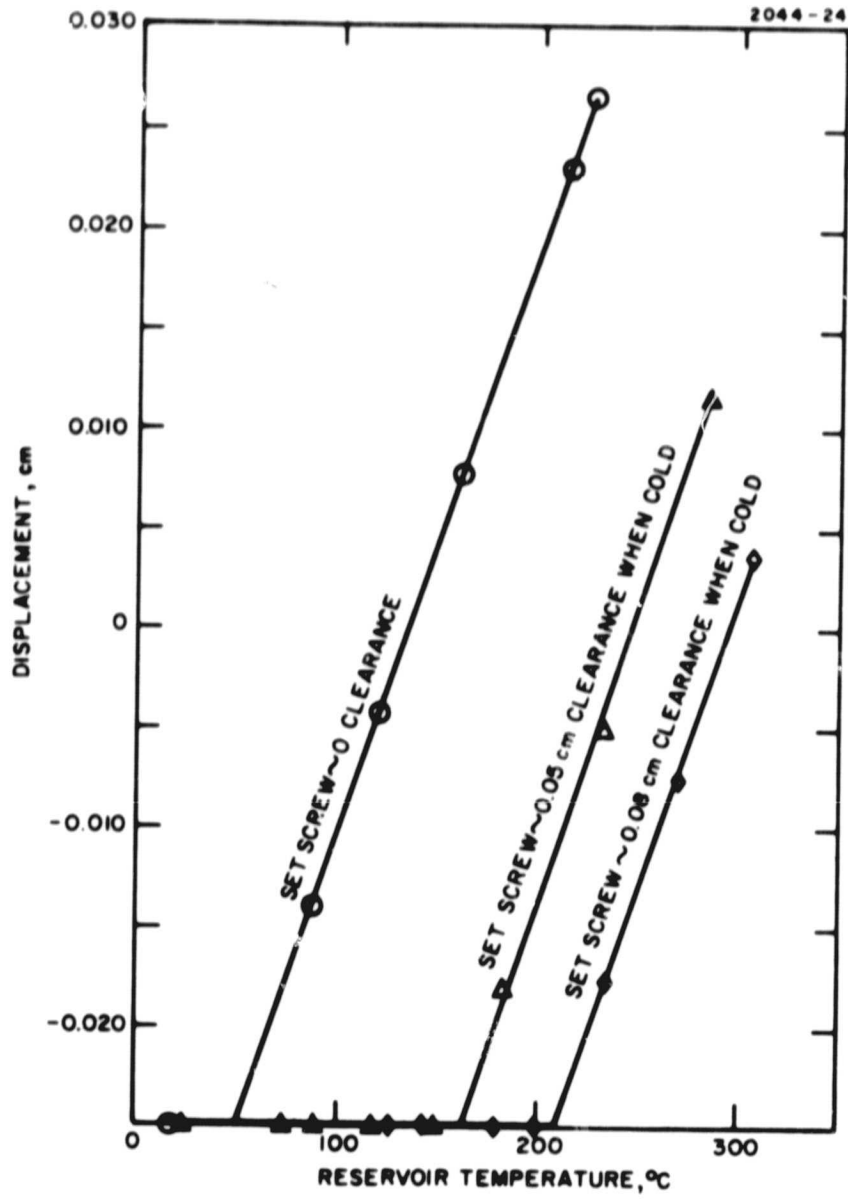


Fig. 27. Extraction SN503 Y-Axis Bench Test.

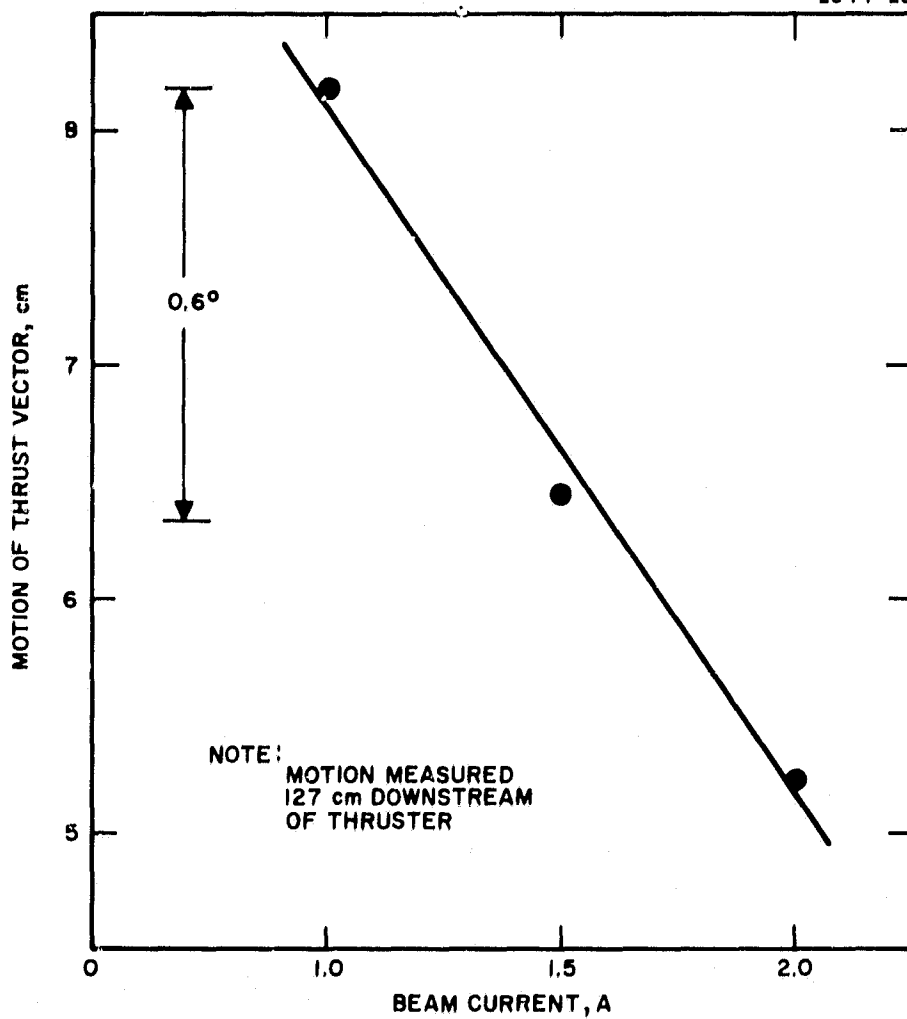


Fig. 28. Thrust Vector Motion as Beam Increases.

temperature ranges from 130 to 178°C, as the beam current is increased to 2.0A. These temperatures are consistent with temperature measurements of the optics support ring reported elsewhere.⁷ The rise in actuator temperature above this ambient is ~37°C/A. of actuator heating current, regardless of beam current. Unfortunately, during these tests, the set point on the accumulator bellows stop was adjusted so this rise in thruster temperature produced a shift in the thrust direction without application of actuator power. The scheduled delivery date did not permit readjustment and further testing to verify that these cross-coupling terms could be eliminated; however, the bench test data shown in Fig. 27 illustrates how this can be done. Figure 28 shows the motion of the thrust vector in a plane 127 cm downstream and perpendicular to the beam direction as the beam is increased. Figure 29 shows the translation in this same plane as the actuators are heated after the ambient temperature has been reached. All slopes are in the range 7 to 8 cm motion/A actuator current.

In terms of angular displacement, the results indicate a value of ~1° deflection for each 0.005 cm of transverse accelerator motion. The maximum deflection angle measured was 9.7° at 2.0 A beam. At this point, the accelerator current was 5.0 mA, which is within experimental error of the nominal value at zero deflection angle, indicating that no direct interception had occurred as a result of this screen electrode motion. A typical beam profile is shown in Fig. 30.

D. CONCLUSION

a. 30-cm Mechanical Thrust Vector System

Two different 30-cm thrust vector systems have been successfully fabricated and tested. Each has demonstrated that the beam can be vectored up to ±10° by moving the screen electrode relative to the accelerator. These tests also have indicated that the total system would be improved by an actuator concept which would shorten the response time and assure that the vector angle is insensitive to both thruster ambient temperature and operating power level.

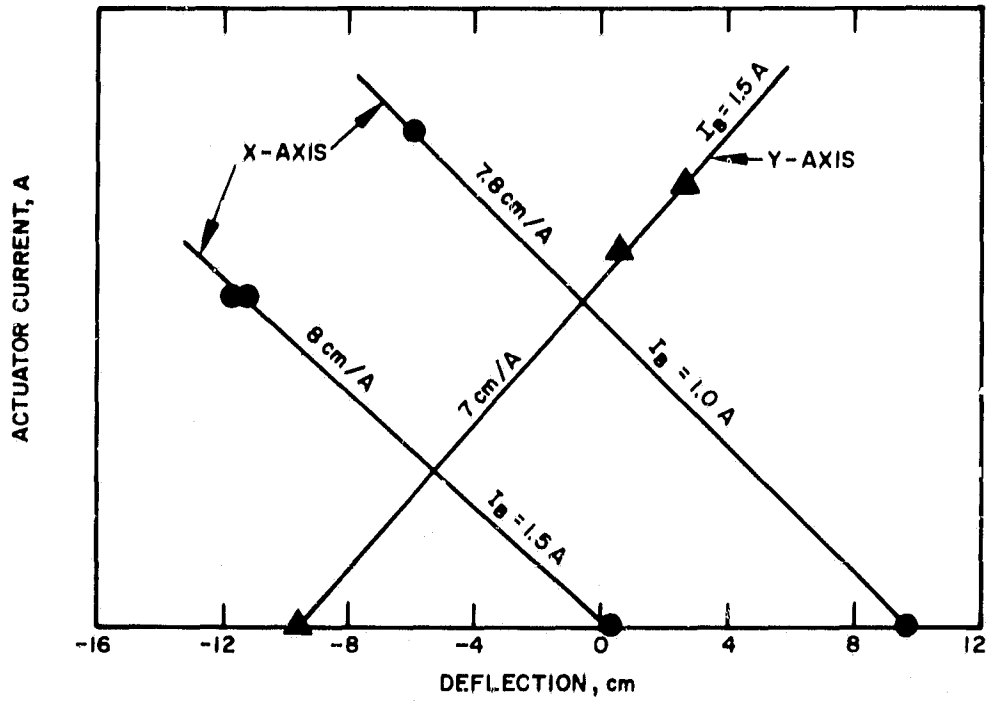


Fig. 29. Results as Actuators are Heated after Ambient Temperature is Reached.

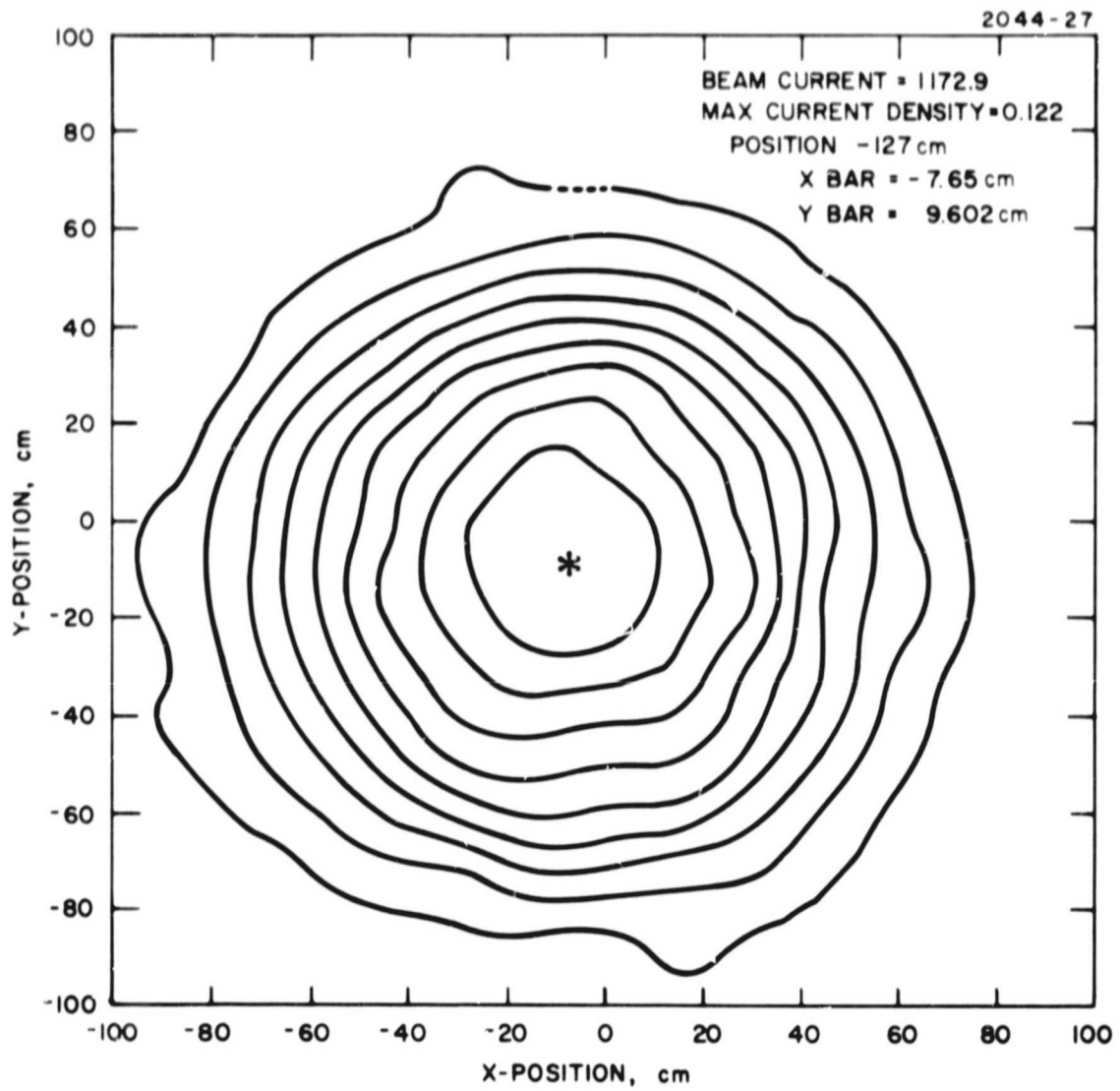


Fig. 30. Typical Beam Profile.

REFERENCES

1. H.J. King and J.H. Molitor, Ion Propulsion — Missions and Technology Proceedings of 21st International Astronautical Conference, 1970.
2. L.B. Holcomb, Satellite Auxiliary Propulsion Technology Technical Report 32-1505, JPL 1971.
3. E. Harvey, V. Lapins, and J. Molitor, Geocentric Solar Electric Propulsion AIAA paper 72-1126, 1972.
4. Low Voltage 30 cm Ion Thruster Development Contract NAS 3-16528, started May 1972 at Hughes Research Laboratories.
5. 2.5 kW Advanced Technology Ion Thruster, Contract NAS 3-16949, started October 1972 at Hughes Research Laboratories.
6. W.C. Latham and W.B. Adams, Theoretical Analysis of a Grid-Translation Beam Deflection System for a 30-cm Diameter Kaufman Thruster, TMX 67911, 1971, NASA LeRC.
7. Hughes Research Laboratories Staff, Monthly Report No. 3 August 1972, Contract NAS 3-16528.

APPENDIX

MEASUREMENT OF BEAMLET SIZE AND SHAPE

In the course of investigating different optics geometries, an interesting technique was used to determine the variation in the beamlets size and shape across the discharge chamber at both the upstream and downstream sides of the deflecting accel electrode. The method used was one that Byers and Banks⁸ used in investigating different grid aperture shapes and it was accomplished by placing thin tantalum foil strips in the apertures and letting the beamlets sputter holes away. Tantalum strips, 0.05-mm thick by 4-mm wide, were placed on both sides of the deflecting accel and were oriented in the vertical and horizontal planes and crossed in the central hole. This experiment was conducted for the configuration 2 and 3 screen geometries (see Table X, Section II), which Ref. 8 showed produced square beamlets. The results of this experiment are illustrated in Fig. 31, which shows the tabulated beam size for grid spacings of 0.076 cm and 0.119 cm. The data is also plotted in Fig. 32. These measurements show the beamlets are almost perfectly square-shaped on the upstream size of the accel electrode, with only a small size variation in the radial direction. The downstream holes do show an appreciable size variation, which indicates the square structure becomes trapezoidal toward the edges. Note that the downstream beam size is smaller for the closer grid spacing, even though the upstream beamlet size is larger for this case. This arises from the fact that the minimum beam size (the beam waist) occurs farther into the deflecting accel for the closer spacing. The optimum condition would occur if the beam waist was halfway down the deflecting accel for the central region holes, which have the largest beam sizes and limit the deflection angle. The beamlet sizes tabulated in Fig. 31 show the beamlets are smaller in the X direction. This probably results from the fact that the notches in the Y strips (which deflect

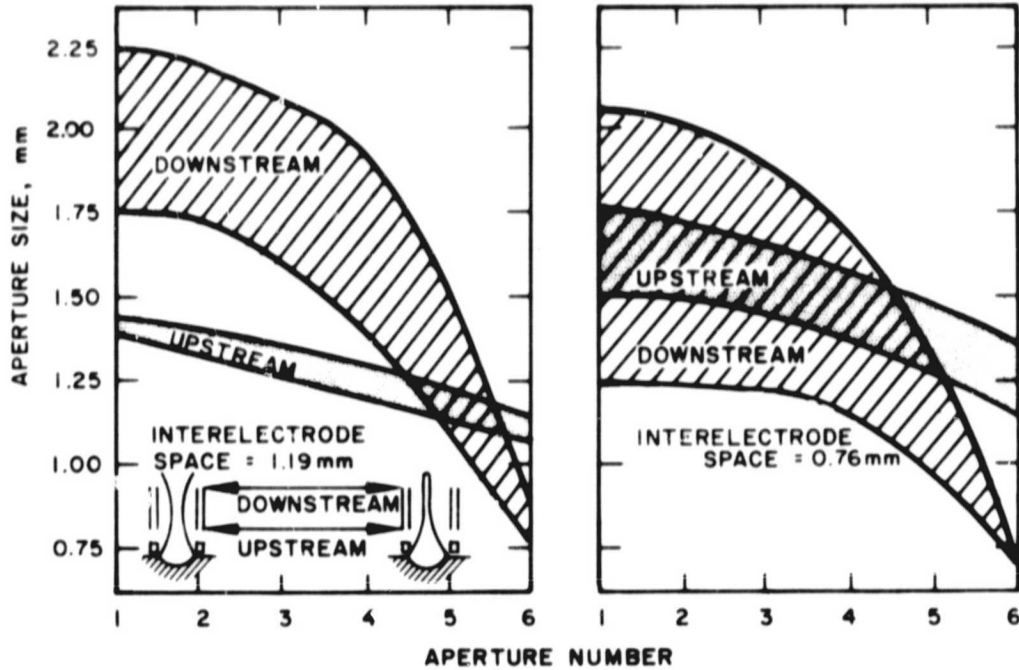


Fig. 32. Measured Beamlet Size Versus Radius for Thrust Vector Optics with Square-Type Screen Apertures for Two Grid Spacings ($I_t \approx 25$ mA, $V_+ = 1200$, $V_- = 1000$ V).

the beam in the X direction) are oriented downstream. This absence of notches facing the plasma boundary in the Y strips evidently provides a stronger converging effect in the X direction with the resulting smaller beam size in this direction. This notch orientation is also responsible for the experimentally measured higher deflection sensitivity in the X direction ($\sim 0.015^\circ/\text{V}$ versus $0.011^\circ/\text{V}$ at 2400 V).